Oriolo Sebastián (Orcid ID: 0000-0002-2495-2431)

The Late Paleozoic tectonometamorphic evolution of Patagonia revisited: Insights from the pressure-temperature-deformation-time (P-T-D-t) path of the Gondwanide basement of the North Patagonian Cordillera (Argentina)

Sebastián Oriolo[a]*, Bernhard Schulz[b], Pablo D. González[c], Florencia Bechis[d], Ezequiel Olaizola[d], Joachim Krause[e], Emiliano M. Renda[a], Haroldo Vizán[a]

[a] CONICET-Universidad de Buenos Aires. Instituto de Geociencias Básicas, Aplicadas y Ambientales de Buenos Aires (IGEBA), Intendente Güiraldes 2160, C1428EHA Buenos Aires, Argentina

[b] Institute of Mineralogy, Division of Economic Geology and Petrology, TU Bergakademie Freiberg, Brennhausgasse 14, D-09596 Freiberg/Saxony, Germany

[c] Instituto de Investigación en Paleobiología y Geología (UNRN-CONICET), Avenida Julio A. Roca 1242, R8332EXZ General Roca, Argentina

[d] Instituto de Investigaciones en Diversidad Cultural y Procesos de Cambio (IIDyPCa), CONICET-Universidad Nacional de Río Negro, Avenida de los Pioneros 2350, R8400AHL San Carlos de Bariloche, Argentina

[e] Helmholtz-Zentrum Dresden-Rossendorf, Helmholtz Institut Freiberg für Ressourcentechnologie, Chemnitzer Str. 40, D-09596 Freiberg/Saxony, Germany

*Corresponding author: seba.oriolo@gmail.com, soriolo@gl.fcen.uba.ar

Key points

- Monazite ages of ca. 300 Ma record peak conditions of 650 °C and 11 kbar achieved during prograde metamorphism and progressive deformation
- Late Paleozoic crustal thickening of Gondwanide basement coeval with forearc metamorphism resulted from a transpressional advancing orogen
- Low-grade metamorphism and transtension at ca. 170 Ma and hydrothermal activity at ca. 100-80 Ma during the onset of Andean transpression

This article has been accepted for publication and undergone full peer review but has not been through the copyediting, typesetting, pagination and proofreading process which may lead to differences between this version and the Version of Record. Please cite this article as doi: 10.1029/2018TC005358

Abstract

Combined field structural analysis with *in situ* EPMA (electron probe microanalysis) Th-U-Pb monazite dating, petrologic and microstructural data provide a reconstruction of the pressure-temperature-deformation-time (P-T-D-t) path of the Gondwanide basement of the North Patagonian Cordillera. For samples from the Challhuaco hill, the timing of development of the metamorphic S_2 foliation and associated L_2 lineation and tight to isoclinal F_2 folds is constrained by monazite ages of 299 ± 8 and 302 ± 16 Ma during peak metamorphic conditions of ca. 650 °C and 11 kbar, achieved during prograde metamorphism and progressive deformation. Metamorphism and deformation of metamorphic complexes of the North Patagonian Andes seem to record Late Paleozoic crustal thickening and are coeval with metamorphism of accretionary complexes exposed further west in Chile, suggesting a coupled Late Devonian-Carboniferous evolution. Instead of the result of continental collision, the Gondwanide orogeny might thus be essentially linked to transpression due to advancing subduction along the proto-Pacific margin of Gondwana. On the other hand, a second generation of monazite ages of 171 ± 9 and 170 ± 7 Ma constrain the timing of low-grade metamorphism related to kink band and F_3 open fold development during Jurassic transtension and emplacement of granitoids. Finally, a Cretaceous overprint, likely resulting from hydrothermal processes, is recorded by monazite ages of 110 ± 10 and 80 ± 20 Ma, which might be coeval with deformation along low-grade shear zones during the onset of Andean transpression.

Keywords: EPMA Th-U-Pb monazite dating, in situ petrochronology, garnet metapelite thermobarometry, Upper Paleozoic, Terra Australis, southwestern Gondwana

1. Introduction

The Late Paleozoic Gondwanide orogen was early recognized in central Argentina by Keidel (1938 and references therein), allowing to establish one of the pioneer geologic correlations across the Atlantic Ocean. However, the tectonic significance of this key orogenic event is still under debate and has been alternatively attributed to subduction, collisional or accretional tectonics (e.g., von Gosen, 2003; Pankhurst et al., 2006; Gregori et al., 2008, 2016; Ramos, 2008; Varela et al., 2015; Vizán et al., 2015, 2017; Hervé et al., 2016; Heredia et al., 2017, 2018). These proposals have in turn led to contrasting hypotheses about the origin of the North Patagonian Massif, for which an allochthonous, autochthonous or para-autochthonous origin has been inferred (Ramos, 1984, 2008; Dalla Salda et al., 1992; Pankhurst et al., 2006, 2014; Gregori et al., 2008; González et al., 2011, 2012, 2018; Rapalini et al., 2010, 2013; Ramos & Naipauer, 2014; Castillo et al., 2017; Heredia et al., 2018).

In the particular case of northwestern Patagonia (Argentina), most contributions focused on the Late Paleozoic magmatism (Cerredo & López de Luchi, 1998; Pankhurst et al., 2006; Urraza et al., 2011; Varela et al., 2005, 2015; Castillo et al., 2017), whereas constraints on the timing and characteristics of contemporaneous deformation and metamorphism are scarce (Fig. 1; Giacosa et al., 2004; von Gosen & Loske, 2004; García-Sansegundo et al., 2009; von Gosen, 2009; Martínez et al., 2012; Urraza et al., 2015). In addition, no clear correlations have been so far established between the igneous-metamorphic basement of the North Patagonian Cordillera/Massif and accretionary complexes exposed further west in Chile in terms of their structural and metamorphic evolution, though the latter record coeval Late Paleozoic sedimentation and subsequent deformation and metamorphism (Martin et al., 1999; Willner et al., 2004; Kato et al., 2008; Hervé et al., 2013). Recently, Hervé et al. (2016, 2018) identified juvenile Devonian magmatism in the accretionary complex of Chile south of 40 °S and thus inferred the Late Devonian-Early Caboniferous accretion of an island arc complex

along the southwestern margin of Gondwana. This hypothesis contrasts significantly with the proposal of Martínez et al. (2012), who suggested the collision of the Chilenia Terrane at ca. 390 Ma, well-documented north of 40 °S (Willner et al., 2011).

On the other hand, a correct understanding of the coupling between deformation and metamorphism is critical for the reconstruction of P-T-D-t paths of deformed metamorphic rocks (Williams & Jercinovic, 2012) and their significance for orogenic evolution. In this sense, combined *in situ* petrologic and microstructural data allow to link deformation mechanisms, metamorphic reactions and macroscopic structural features and to infer the relative timing of different mineral associations and microstructures (Johnson, 1999; Marsh et al., 2009; Hobbs et al., 2011; Skrzypek et al., 2011; Goncalves et al., 2012; Yakymchuk & Godin, 2012; Oriolo et al., 2018). The absolute timing of deformation and metamorphism, in turn, can be constrained by interpreting *in situ* geochronologic data in the light of microstructures, which provide insights into mineral equilibria, deformation mechanisms and metamorphic reactions (Mulch & Cosca, 2004; Tchato et al., 2009; Williams & Jercinovic, 2012; Villa et al., 2014; Gasser et al., 2015; Oriolo et al., 2016a, 2018; Schulz, 2017; Bosse & Villa, 2019). Furthermore, the integration of structural, microstructural, petrologic and geochronologic data permits reconstructing the crustal architecture of orogens and contributes on the understanding of their tectonic and geodynamic evolution (e.g., Goscombe & Gray, 2009; Raimondo et al., 2010; Endo & Wallis, 2017).

In this contribution, new structural, microstructural, petrologic and EPMA Th-U-Pb monazite data from gneisses and schists of basement rocks of the North Patagonian Cordillera (southwestern Argentina) are shown, providing a reconstruction of the P-T-D-t path of the Gondwanide basement of the study area. Based on these results, a revised model for the tectonic evolution of northern Patagonia is presented, providing insights into the coupled evolution of the igneous-metamorphic basement of North Patagonian Cordillera/Massif and accretionary

complexes of Chile, and the Late Paleozoic configuration of the southwestern Gondwana margin. In addition, geochronologic and structural constraints on the Mesozoic tectonic evolution of the North Patagonian Cordillera are included as well, based on the Jurassic-Cretaceous record of basement rocks.

2. Regional setting

The North Patagonian Cordillera (southwestern Argentina) is located at the southern segment of the Central Andes and is bounded to the west and east by the Central Valley of Chile and the North Patagonian Massif, respectively (Fig. 1). This morphostructural unit comprises an Andean thick-skinned fold and thrust belt and is essentially made up of Paleozoic igneous-metamorphic rocks, Mesozoic granitoids and subordinated volcano-sedimentary rocks, and Cenozoic volcano-sedimentary sequences and granites (González Díaz, 1982; Rapela et al., 1988; Dalla Salda et al., 1991; Giacosa et al., 2001, 2005; Giacosa & Heredia, 2004; Castro et al., 2011a; Bechis et al., 2014a; Iannelli et al., 2017).

In the study area, located to the south of the Nahuel Huapi lake (Fig. 2), the basement is considered to be part of the Colohuincul Complex (Dalla Salda et al., 1991) and comprises mostly paragneisses and schists with subordinated intercalations of amphibolites, metarhyolites, felsic orthogneisses and foliated intrusions (Dalla Salda et al., 1991; García-Sansegundo et al., 2011). A structural characterization was presented by Dalla Salda et al. (1991) and García-Sansegundo et al. (2009), though quantitative structural data are still scarce. Martínez et al. (2012) obtained EPMA Th-U-Pb monazite ages of 391.7 ± 4.0 and 350.4 ± 5.8 Ma for migmatitic paragneisses near the Brazo Tronador, interpreted as the timing of peak and retrograde metamorphic conditions, respectively. For these rocks, metamorphic conditions of ca. 612 °C and 4.9 kbar were determined. In addition, high-pressure metamorphism with peak

conditions of ca. 440 °C and 18 kbar were calculated for a garnet-bearing micaschist exposed at the southern margin of the Gutiérrez lake (Martínez et al., 2012). In this area, detrital zircons of metasedimentary rocks yield Early Paleozoic maximum sedimentation ages (Hervé et al., 2018).

Deformation and metamorphism of basement rocks of the North Patagonian Cordillera and the western North Patagonian Massif have been interpreted as the result of Late Paleozoic compression/transpression during the Gondwanide Orogeny (Giacosa et al., 2004; García-Sansegundo et al., 2009; von Gosen, 2009). Within this framework, rocks of the study area were assigned to a hinterland position (García-Sansegundo et al., 2009). In contrast, Martínez et al. (2012) inferred a forearc setting for these rocks, associated with an older, Devonian collisional event, as recorded north of 40 °S (Willner et al., 2011). The validity of this model was, however, questioned by Hervé et al. (2016, 2018). These authors proposed a Late Devonian-Early Carboniferous accretion of an island arc complex, considering igneous-metamorphic basement rocks of the North Patagonian Cordillera and the western North Patagonian Massif as remnants of a Devonian continental arc.

On the other hand, the Jurassic record of the study area is characterized by granitoids of the Cordilleran batholith yielding U-Pb SHRIMP zircon crystallization ages of ca. 176-160 Ma (Castro et al., 2011a) and scarce volcano-sedimentary sequences (Giacosa et al., 2001). Based on pluton fabrics, Castro et al. (2011a) inferred regional sinistral strike-slip deformation, thus contrasting with the Middle-Late Jurassic extensional regime recorded by extensional structures of volcanic rock depocenters of the North Patagonian Cordillera located further south (Echaurren et al., 2016, 2017).

Finally, Cretaceous to Cenozoic rocks of the North Patagonian Cordillera are intimately related to Andean tectonics, with two main Middle-Late Cretaceous and Miocene orogenic

phases (Orts et al., 2012; Gianni et al., 2018; Horton, 2018). In contrast to the Miocene transpressional phase, which is well-recorded by structural, kinematic and geochronologic data of volcano-sedimentary and granitic rocks (Diraison et al., 1998; Giacosa et al., 2001, 2005; Giacosa & Heredia, 2004; Orts et al., 2012; Bechis et al., 2014a), the Cretaceous Andean record of the study area is only restricted to few granitoids yielding K-Ar and Rb-Sr ages of ca. 120-80 Ma (González Díaz, 1982, and references therein). However, coeval thrusting was reported in adjacent regions of northwestern Patagonia (Orts et al., 2012; Echaurren et al., 2016, 2017; Gianni et al., 2018).

3. Methodology

Field mapping and structural analysis were applied in different exposures of the igneous-metamorphic basement of the North Patagonian Cordillera south of the Nahuel Huapi Lake (Fig. 2), where samples were also collected for microstructural, geochronologic and thermobarometric analysis. EPMA Th-U-Pb monazite data combined with SEM-based automated mineralogic methods were obtained in three samples of metasedimentary rocks (BA 20-17, BA 22-17 and BA 11-18). Sample descriptions and locations are presented in Text S1 in the Supporting Information, whereas analytical details are provided in Text S2 in the Supporting Information. In addition, thermobarometry was applied in sample BA 22-17 in order to quantify pressure-temperature metamorphic conditions (Text S2 in the Supporting Information; Powell & Holland, 1994, 2008).

4. Results

4.1. Structure

The most conspicuous macroscopic fabric element is a metamorphic S_2 foliation (Fig. 2), though relics of bedding planes S_0 and a metamorphic S_1 foliation are occasionally observed as well (Figs. 3a, 3b). S_1 represents an axial plane foliation of isoclinal F_1 folds affecting S_0 planes, whereas S_2 represents an axial plane foliation of tight to isoclinal F_2 folds that fold S_1 (Fig. 3c), which is clearly observed at the microscale (see Section 4.2). Rootless F_2 hinges are common, being defined by folded quartz segregations, and in some cases, F_2 folds are superimposed to isoclinal F_1 folds (Fig. 3d). The orientation of S_2 planes is variable, despite showing a dominant NNW-SSE to WNW-ESE strike (Fig. 3b). A stretching lineation L_2 defined by shape-preferred orientation of micas and/or staurolite is associated with S_2, exhibiting subhorizontal plunges towards NNW-SSE to WNW-ESE, which is parallel to the strike of S_2 planes in most cases (Fig. 2).

Kink bands and late gentle to open F_3 folds affecting S_2 are also present exhibiting, in many cases, a kink geometry (Fig. 3e, 3g). Though variable, F_3 axial planes strike dominantly NE-SW and exhibit subvertical to steep dip towards SE. Fold hinge lines, in turn, show moderate plunge towards ENE and E. A spaced S_3 foliation is occasionally observed as an axial plane foliation of F_3. On the other hand, a mylonitic S_3' foliation is also developed within low-grade shear zones (Fig. 3f), comprising mostly ultramylonites, phyllonites and pseudotachylites. Field relationships between kink bands and shear zones are not exposed. In some cases, a crenulation cleavage is associated with the mylonitic foliation, being localized within shear zone lozenges (Fig. 3h), whereas a cataclastic overprint is observable as well.

The schematic structural profile of Figure 4 summarizes the relationship of different structural elements for the western margin of the Jakob lake (Fig. 2). In this case, S_2 planes

strike dominantly NNW-SSE and dip steeply towards ENE, whereas L_2 lineations plunge gently towards SSE. Tight to isoclinal F_2 folds have subvertical hinge lines. Conjugated subvertical NE-SW- and NW-SE-striking kink bands exhibit subvertical axes. In a similar way, subvertical low-grade ductile to brittle-ductile S_3' shear zones strike dominantly NE-SW to NNE-SSW and show a dextral sense of shearing.

4.2. Microstructures

Schists are mostly made up of muscovite + biotite + quartz + plagioclase and characterized by the S_2 foliation, which typically comprises a spaced schistosity. Schistosity domains are mostly made up of muscovite and subordinated biotite, whereas microlithons encompass quartz and, to a minor extent, plagioclase. S_2 is commonly observed as a crenulation schistosity, due to the presence of relics of folded S_1 planes in the microlithons of S_2 (Fig. 5a). In turn, S_1 is characterized by muscovite + quartz + biotite ± plagioclase. In addition, garnet and plagioclase porphyroblasts are frequently observed in the metapelitic schists (Fig. 5b). Staurolite, K-feldspar and sillimanite are occasionally present as well. Monazite, rutile, tourmaline, zircon, apatite and titanite are accessory minerals.

Muscovite and biotite present shape-preferred orientation parallel to S_1 and S_2 planes, whereas quartz shows granoblastic microstructures and, in some cases, chessboard extinction (Fig. 5c). Garnet and plagioclase porphyroblasts commonly exhibit inclusion trails defining folded S_1 planes and strain shadows (muscovite + quartz + biotite + plagioclase ± garnet) of S_2 planes (Figs. 5b, 5d), suggesting a syn-S_2 crystallization during folding (i.e., F_2) of S_1. Some syn-S_2 garnet porphyroblasts are also revealed by the presence of an internal rotated foliation that resembles S_2 (Fig. 5e). In a similar way, a syn-S_2 growth of plagioclase porphyroblasts is indicated by trails of inclusions that are parallel to S_2 (Fig. 5f).

Chlorite and fine-grained white mica are retrograde minerals replacing garnet, biotite and plagioclase. Both minerals form fine-grained aggregates with shape-preferred orientation parallel to S_2, which is locally affected by mikrokinking or crenulation (Fig. 5g; Text S1 in the Supporting Information). When present, S_3 corresponds to a crenulation cleavage.

Finally, ultramylonites and phyllonites of S_3' shear zones are made up of scarce porphyroclasts of plagioclase, muscovite and opaque minerals immersed in a fine-grained matrix of quartz + chlorite + muscovite + biotite + opaque minerals. In the matrix, quartz is mostly restricted to granoblastic monomineralic layers, indicating post-shearing recovery, whereas mica layers typically exhibit grain shape-preferred orientation and local concentration of opaque minerals in trails parallel to the mylonitic foliation (Fig. 5h), suggesting the role of dissolution-precipitation. Microstructures suggest that strain was mostly accommodated along mica-rich layers, with dissolution-precipitation as the main deformation mechanism, though subordinated bulging recrystallization was locally observed in quartz. However, evidence of cataclasis overprinting mylonitic features are common, with microfractures filled with fine-grained epidote + chlorite + white mica + quartz.

4.3. Mineral chemistry and thermobarometry

Garnet, white mica, biotite, plagioclase and chlorite compositions in the garnet-bearing metapelite of sample BA 22-17 were determined. Analytic methods and results are provided in Text S1 in the Supporting Information and Table S1 in the Supporting Information, respectively.

Compositional zonation of garnets of up to 7 mm diameter were determined using the GXMAP mode of automated SEM (Fig. 6a). The garnet mineral chemical evolution was then detailed by EPMA analyses along profiles. In the porphyroblasts, the spessartine (Mn) contents

decrease from ~9 to 1 mol % and the pyrope (Mg) contents increase from 3 to 11 mol % from core to rim, corresponding to a typical prograde zonation (Spear, 1993). The grossular (Ca) contents decrease from 28 to 10 mol %, whereas almandine increases from 60 to 77 mol %. In addition, a decrease of *X*Ca from 0.27 to 0.05 and an increase of *X*Mg from 0.03 to 0.14 are observed from cores to rims. Garnet outer rims display no significant increase of Mn and Ca. Unaltered biotite are rarely preserved in the micaschists and could be analyzed only when enclosed in plagioclase and quartz. According to their angular structural orientation in reference to the main foliation S_2, these biotites should be considered as S_1 biotites. They have a X_{Mg} of ca. 0.46, with Ti of ca. 0.13 and ^{IV}Al of ca. 0.18 (p.f.u.). Biotites in the main foliation S_2 are mostly altered into chlorite, with totals below 92 wt. %. Their X_{Mg} is ca. 0.52, with similar Ti and ^{IV}Al as the S_1 biotites. As biotite, the muscovite appears in the S_1 microstructural position, mostly oblique to the main foliation S_2. Their Si^{4+} contents around 3.18 (p.f.u.) do not differ among different microstructural positions, similarly to Na (ca. 0.26-0.28 p.f.u.) and Mg (ca. 0.06-0.08 p.f.u.) contents. On the other hand, chlorite appears in various microstructural positions (Text S1 in the Supporting Information). Along the margins of the garnet, replacement of garnet by chlorite is observed, with X_{Mg} of 0.52 at ^{IV}Al of 2.58 and ^{VI}Al of 2.75 (p.f.u.). Along S_2 planes, the chlorite replaces the biotite at variable degrees, which led to X_{Mg} of 0.38-0.52, ^{IV}Al of 2.23-2.58 and ^{VI}Al of 2.73 (p.f.u.). Inclusions of plagioclase in the garnet porphyroblast are unzoned oligoclase and have anorthite contents between ca. 15 and 20 mol %. In the matrix along the foliation and next to the garnet margins, the small oligoclases are also unzoned but with lower anorthite contents between 11 and 15 mol %. Large plagioclase porphyroblasts in S_2 microlithons, which enclose crenulated S_1, show the same variation in anorthite contents. In general, a trend toward slightly lower Ca contents during plagioclase crystallization can be defined.

The garnet crystallized with a low-variance assemblage of biotite, muscovite,

plagioclase and quartz. These phases occur as aligned inclusions in the garnet porphyroblasts, and also along S_1 and S_2 foliations. Rutile and ilmenite also occur in garnet porphyroblasts and in the foliated matrix. In terms of the garnet X_{Mg}-X_{Ca} evolution (Spear, 1993), the garnet zonation semiquantitatively corresponds to a prograde metamorphism, with an initial increase of both pressure and temperature. The strong decrease of Ca toward the garnet rim signals subsequently decreasing pressure. Such a relative $\Delta P/\Delta T$ trend appears to be mainly preserved when uncertainties about the corresponding plagioclase and biotite are considered (Spear, 1993).

Pressure and temperature for crystallization of garnet core were calculated by the calibrations of Holdaway (2000) and Wu (2015), involving enclosed plagioclase An_{17} and mica in the relic S_1 foliation. This yielded ca. 400-450 °C at 7 kbar, with a slight dependency of the chosen biotite and plagioclase composition. A minimum error of ±50 °C and ±1 kbar has to be considered for each equilibrium calculation. Calculations for the middle parts of the garnet zonation profile with increased Mg contents, considering the composition of S_1 biotites, led to higher temperatures and pressures. Peak conditions were calculated from garnet inner rims with 10 mol % grossular combined with matrix An_{15} plagioclase, yielding ca. 650 °C at 11 kbar (Fig. 6b). A significant decrease of the grossular (Ca) content to 5 mol % towards the outer garnet rim resulted in a pressure drop to ca. 8 kbar for the final stage of the garnet crystallization during nearly isothermal conditions. The single P-T estimates from the zoned garnet define a clockwise P-T path within the kyanite stability field (Fig. 6b). Alternative calculations with other thermobarometers and the av*PT* routine (Powell and Holland, 1994) yielded comparable results. After the P-T record of the garnet-bearing assemblage, a retrograde evolution with further decrease of pressure and temperature can be expected, as recorded by temperature of ca. 335 °C calculated from chlorite thermometry. As the P-T path enters the monazite stability field for low-Ca bulk-rock compositions during decreasing pressure (Spear, 2010), monazites

might start to grow at or shortly after peak conditions.

4.4. Monazite dating and mineral chemistry

In the case of garnet micaschists of the Challhuaco hill, a population of high-Th+U monazites in samples BA 20-17 and BA 22-17 yield nearly identical Late Pennsylvanian ages of 299 ± 8 and 302 ± 16 Ma, respectively (Fig. 7). Likewise, sample BA 20-17 presents a low-Th+U monazite age population of 80 ± 20 Ma, whereas a low-Th+U monazite age population of sample BA 22-17 exhibits an age of 171 ± 9 Ma. The latter is comparable to the Middle Jurassic age recorded by sample BA 11-18, collected at the Jakob lake, which also yields a Cretaceous age of 110 ± 10 Ma. Further analytic results are provided in Table S2 in the Supporting Information. Carboniferous monazites are typically large and almost lack in sutured grain boundaries. In contrast, Jurassic and Cretaceous monazites are smaller and show severely sutured grain boundaries and sponge-like microstructures, being also associated with fine-grained chlorite and white mica (Fig. 7). The lack of Carboniferous monazites in sample BA 11-18 can be explained by the Ca bulk rock composition. The calculated values obtained from the automated SEM modal analysis of this sample indicate a considerably higher bulk rock Ca content (1.3 wt. %) than samples BA 20-17 and BA 22-17 (0.7 and 0.52 wt. %, respectively).

Monazite chemical composition support a discrimination of age populations (Fig. 8). Carboniferous monazites yield relatively homogeneous Y_2O_3 contents, with most values between ca. 0.8 and 1.2 wt. % (Fig. 8a). In spite of their similar ages, Jurassic monazites of samples BA 22-17 and BA 11-18 show differences, with Y_2O_3 contents that are lower or higher than a threshold value of ca. 1 wt. %, respectively. The Y_2O_3 content of Cretaceous monazites, in turn, varies between ca. 0.2 and 1.2 wt. %. On the other hand, Carboniferous monazites present comparable X_{YPO4} and X_{GdPO4} contents between ca. 0.018 and 0.024 (Fig. 8b). All

Jurassic monazites show X_{GdPO4} contents higher than 0.016, though sample BA 11-18 shows X_{YPO4} contents higher than those of sample BA 22-17. X_{YPO4} and X_{GdPO4} of the latter are relatively similar to those of Cretaceous monazites. Carboniferous and Jurassic monazites of sample BA 11-18 exhibit a positive correlation in the Th + U vs Ca plot, with Ca contents mostly higher than 0.1, as in the case of Cretaceous monazites (Fig. 8c). In contrast, Jurassic monazites from sample BA 22-17 yield Ca contents lower than 0.1. Both Carboniferous and Jurassic monazites of the Jakob lake show low Si contents (<0.15), whereas Cretaceous and Jurassic monazites of sample BA 22-17 exhibit values up to ca. 0.25 (Fig. 8d). The latter also show a positive correlation between Th + U and Si. Carboniferous monazites show the highest UO_2 contents (>0.62 %). Likewise, relatively high UO_2 contents are observed for Jurassic monazites of sample BA 11-18 (ca. 0.24-0.8 wt. %), thus showing a significant difference with low UO_2 contents of Cretaceous and Jurassic monazites of sample BA 22-17 (Fig. 8e). In sum, Carboniferous and Jurassic ages are the most abundant groups in the monazite age distribution pattern, though a subordinated Cretaceous population is also well-recorded (Fig. 8f).

5. Discussion and interpretation

5.1. P-T-D-t path of the Gondwanide basement

The ubiquitous S_2 foliation shows a dominant WNW-ESE to NNW-SSE strike (Figs. 2, 3), as reported by Dalla Salda et al. (1991) and García-Sansegundo et al. (2009). In a similar way, stretching lineations L_2 exhibit subhorizontal to gentle plunge to the NNW-SSE or WNW-ESE (Figs. 2, 4). Structural data point to bulk inclined transpression (Jones et al., 2004), with partitioning into strike-slip- and contraction-dominated domains suggested by differences in the orientation of S_2, L_2 and F_2 (Figs. 2, 4). Subvertical to steeply dipping S_2 and F_2 axial planes, steeply dipping F_2 hinges and gently plunging L_2 lineations (e.g., Jakob lake and Paso de las

Nubes) may record the former, whereas the latter may be registered by moderately to gently dipping S_2 and F_2 axial planes, and gently dipping F_2 hinges subparallel to gently plunging L_2 lineations (e.g., Ñireco and Challhuaco hills). Alternatively, such differences may arise from subsequent modifications due to Mesozoic and Cenozoic tectonic processes, which significantly overprinted the area (e.g., Giacosa & Heredia, 2004; Castro et al., 2011a; Bechis et al., 2014a). Local variations are observed in the structural profile between the Témpanos and Jakob lakes (Fig. 4), where significant post-Paleozoic deformation is absent. In the Paso de las Nubes area (Fig. 2), on the other hand, the presence of Jurassic volcano-sedimentary rocks overlying the basement suggests the lack of post-Jurassic tilting, thus indicating a relative preservation of the orientation of basement fabrics (i.e., subvertical to steeply dipping S_2 and subhorizontal to gently plunging L_2), though vertical axis rotations cannot be discarded.

The garnet-bearing mineral assemblage of the Challhuaco hill schist records a first section of a prograde P-T path under conditions outside the monazite stability field, even for low bulk rock Ca compositions (Fig. 6b). Crystallization of monazite can thus be expected at peak metamorphic conditions (ca. 650 °C and 11 kbar) and mostly during subsequent decompression. In consequence, the Carboniferous monazite population will mark the minimum age for most of the prograde syn-S_1-S_2 amphibolite facies event. Since monazites lie parallel to S_2, the timing of S_2-L_2 and associated F_2 fabrics is constrained by EPMA Th-U-Pb monazite ages of 299 ± 8 and 302 ± 16 Ma (Fig. 6), roughly coeval or slightly younger than peak metamorphic conditions of ca. 650 °C and 11 kbar. Since S_1 and S_2 share structural and microstructural features (e.g., isoclinal folding), it can thus be inferred that S_1-F_1 may be Carboniferous in age as well. According to microstructural evidence (Fig. 6a), S_1-F_1 may be related to prograde metamorphism developed prior to peak metamorphic conditions, being the evolution from S_1-F_1 to S_2-F_2 the result of progressive transpressional deformation (Carreras & Druguet, 2018; Fossen et al., 2018).

On the other hand, late deformation fabrics (i.e., kink bands, F_3 open folds, shear zones) record low-grade metamorphic conditions. Kink bands and open folds are commonly associated with widespread crystallization of fine-grained chlorite and white mica (Section 4.2; Text S1 in the Supporting Information; García-Sansegundo et al., 2009), for which mean temperature conditions of ca. 335 °C were calculated from chlorite thermometry (Section 4.3). In shear zones, mineral associations and microstructures suggest peak deformation conditions of ca. 350-300 °C, though evidence of late cataclasite and pseudotachylite development suggests further deformation below brittle-ductile transition conditions up to ca. 200-150 °C (Fagereng & Toy, 2011; Wallis et al., 2015; Wehrens et al., 2016). Despite being previously interpreted as the result of the final stages of the Gondwanide orogeny (García-Sansegundo et al., 2009), new evidence suggests a post-Paleozoic age for all these younger structures (see below). The pervasive crystallization of new monazite with low Th + U contents during a wide time span during the Mesozoic suggests that associated deformation fabrics under retrograde metamorphic conditions might take place at considerably lower pressures than Carboniferous events (Fig. 6b).

Comparison of P-T-D-t data obtained herein with previous P-T-t data from Martínez et al. (2012) suggests some differences among basement blocks in the study area in terms of P-T evolution and timing of metamorphism. Martínez et al. (2012) reported EPMA Th-U-Pb monazite ages of 391.7 ± 4.0 and 350.4 ± 5.8 Ma at the Brazo Tronador, for which metamorphic conditions of ca. 612 °C and 4.9 kbar were determined. In addition, conditions of ca. 440 °C and 18 kbar were determined for schists at the southern margin of the Gutiérrez lake (Martínez et al., 2012), but the timing of this high-pressure metamorphic event still remains elusive. Instead of a common P-T-D-t path (Dalla Salda et al., 1991; García-Sansegundo et al., 2009), basement blocks south of the Nahuel Huapi lake thus record different parts of a more complex long-term tectonometamorphic evolution, extending at least from ca. 390 to 300 Ma (see also

Section 5.2). Hence, these rocks underwent not only deformation and metamorphism related to the Gondwanide orogeny, which is restricted to the Carboniferous-Permian (e.g., Pankhurst et al., 2006; Heredia et al., 2017, 2018), but also to pre-Gondwanide Devonian tectonometamorphic processes.

5.2. Implications for the Late Paleozoic evolution of northern Patagonia

Basement rocks exposed to the south of the Nahuel Huapi lake have been traditionally ascribed to the Colohuincul Complex (Dalla Salda et al., 1991; Giacosa et al., 2001; García-Sansegundo et al., 2009; Martínez et al., 2012), which was defined by Turner (1965) to nucleate isolated outcrops of low-grade schists, quartzites and phyllites exposed in the northernmost North Patagonian Cordillera and the Southern Neuquén Precordillera at ca. 39° S. Both lithotypes and metamorphic grade in the *locus typicus* of the Colohuincul Complex contrast significantly with those of the study area (Sections 2, 4.3; García-Sansegundo et al., 2009; Martínez et al., 2012). In addition, metasedimentary rocks of the Colohuincul Complex were correlated with those of the Cushamen Formation (Cingolani et al., 2011, and references therein), which may have a late Carboniferous deposition age (Hervé et al., 2005; Marcos et al., 2018), being thus incompatible with Middle Devonian to Carboniferous ages of metamorphism reported for the study area (Section 4.4; Martínez et al., 2012). For this reason, the Bariloche Complex is proposed as a new stratigraphic unit to include basement rocks exposed to the south of the Nahuel Huapi lake, which record Devonian-Carboniferous metamorphism and Early Paleozoic maximum deposition ages (Hervé et al., 2018).

On the other hand, EPMA Th-U-Pb monazite ages of ca. 300 Ma (Section 4.4) constrain the timing of deformation and metamorphism linked to the development of ubiquitous NNW-SSE- to WNW-ESE-striking S_2 and associated L_2 and F_2 fabrics (Section 5.1). Comparable

NW-SE- to NNW-SSE-striking fabrics were also reported for medium-grade basement rocks of the western North Patagonian Massif, where foliated late Carboniferous intrusions occur as well (Cerredo & López de Luchi, 1998; Giacosa et al., 2004; Pankhurst et al., 2006; von Gosen, 2009; García-Sansegundo et al., 2009; Renda et al., 2017). Furthermore, metasedimentary rocks recording Upper Devonian-Carboniferous low-grade metamorphism of the Northern and Southern Neuquén Precordillera (Fig. 1) also exhibit NW-SE- to NNW-SSE-striking foliations (Franzese, 1993, 1995; Zappettini et al., 2012).

The timing of metamorphism and associated deformation of the basement in northwestern Patagonia is mostly constrained at ca. 390-300 Ma (Fig. 1), being thus comparable to the Devonian to Lower Permian ages of associated intrusions (Fig. 9a; Varela et al., 2005; Pankhurst et al., 2006; López de Luchi & Cerredo, 2008). EPMA monazite ages of 391.7 ± 4.0 and 350.4 ± 5.8 Ma were obtained in migmatitic paragneisses near the Brazo Tronador (Martínez et al., 2012), whereas a U-Pb titanite age of 380 ± 2 Ma was reported for a calc-silicate gneiss close to Piedra del Águila (Lucassen et al., 2004). Late Devonian metamorphism is evidenced by comparable ages of 360 ± 7 (EPMA Th-U-Pb monazite; Urraza et al., 2008) and ca. 359 Ma (U-Pb titanite data; Varela et al., 2005) reported further north in the North Patagonian Cordillera and Southern Neuquén Precordillera, respectively. In addition, Devonian to Carboniferous metamorphic overgrowths were reported in zircon grains from metasedimentary rocks at the Gutiérrez lake margin (Hervé et al., 2018) and El Maitén gneiss (Pankhurst et al., 2006), whereas whole-rock K-Ar ages of ca. 380-300 Ma roughly constrain the timing of greenschist facies metamorphism of the Piedra Santa Complex in the Southern Neuquén Precordillera (Franzese, 1995).

Geochemical data of Devonian to Permian magmatic rocks spatially associated with basement inliers show a progressive increase of Sr/Y from the Devonian to the Lower Permian (Varela et al., 2005, 2015; Pankhurst et al., 2006), which may result from increasing crustal

thickness (Fig. 9a; Chapman et al., 2015; Chiaradia, 2015; Profeta et al., 2015). This is consistent with the crustal thickening event suggested by Cerredo & López de Luchi (1998) for this Late Paleozoic magmatism. P-T-t data of the basement show a similar trend, with younger ages of metamorphism for higher pressure peak metamorphic conditions (Sections 4, 5.1; Martínez et al., 2012; Serra-Varela et al., 2017, 2018), although this trend could alternatively be explained by differential exhumation. Nevertheless, a progressive crustal thickening is further supported by the prograde P-T path of the Challhuaco sample (Fig. 6). Peak P-T conditions and the relatively low geothermal gradient recorded during prograde metamorphism (ca. 10-20 °C/km, Fig. 6) together with coeval intrusions at ca. 330-300 Ma located immediately south (Varela et al., 2005, 2015; Pankhurst et al., 2006) suggest a position close to the arc-forearc transition in a Carboniferous continental arc setting for the Challhuaco schists (Fig. 9b).

Ages of metamorphism recorded in accretionary complexes of Chile between ca. 390-300 Ma are coeval with ages of metamorphism recorded in the metamorphic basement of the North Patagonian Cordillera and the western North Patagonian Massif (Figs. 1, 9a), accounting for a common evolution of all these areas, further supported by similarities in the orientation of NNW-SSE- to WNW-ESE-striking metamorphic foliations related to transpression (Fig. 2; Martin et al., 1999; Duhart et al., 2001). In the high P/T Western Series at ca. 41°S (Fig. 1), a $^{40}Ar/^{39}Ar$ hornblende plateau age of 361.0 ± 1.7 Ma in a garnet-bearing amphibolite of Los Pábilos boulders provides a minimum age for eclogite to epidote-amphibolite facies metamorphism at ca. 555 °C and >13 kbar (Kato et al., 2008), comparable to peak metamorphic conditions of ca. 600-760 °C and 11.0-16.5 kbar estimated by Willner et al. (2004) for these rocks. The age of subsequent retrograde blueschist facies metamorphism at ca. 350-500 °C and 10-14 kbar is constrained at 305.3 ± 3.2 and 296.6 ± 4.7 Ma by Rb-Sr mineral isochron data from garnet-bearing amphibolites and schists, respectively (Willner et al., 2004). A slightly

older $^{40}Ar/^{39}Ar$ muscovite age of 325.0 ± 1.1 Ma was also reported for this event (Kato et al., 2008). On the other hand, K-Ar and $^{40}Ar/^{39}Ar$ muscovite ages of ca. 390-370 Ma from borehole samples of schists, further supported by an $^{40}Ar/^{39}Ar$ hornblende inverse isochron age of 359.3 ± 4.4 Ma of an undeformed granitic intrusion, indicate Devonian metamorphism for the Llanquihue Basement Complex (Fig. 1; McDonough *apud* Quezada, 2015; Hervé et al., 2016).

The tectonometamorphic evolution of the Gondwanide basement and associated intrusions seem thus to record progressive crustal thickening related to a Late Paleozoic continental magmatic arc (Varela et al., 2015; Hervé et al., 2016). However, Martínez et al. (2012) suggested a Devonian collision of the Chilenia terrane as the most likely trigger for deformation and metamorphism of rocks of the North Patagonian Cordillera. This interpretation is based on the peak metamorphic conditions of ca. 440 °C and 18 kbar calculated for a garnet-bearing micaschist exposed at the southern margin of the Gutiérrez lake and the EPMA Th-U-Pb monazite age of 391.7 ± 4.0 Ma recorded by a migmatitic paragneiss of the Brazo Tronador. Since the latter also yielded peak metamorphic conditions of ca. 612 °C and 4.9 kbar, the Devonian monazite age cannot be ascribed to high-P/low-T metamorphism but, instead, seem to be associated with low-P/high-T conditions. In contrast to the collisional model of Martínez et al. (2012), Hervé et al. (2016, 2018) proposed the Late Devonian-Early Carboniferous accretion of an island arc complex. Nevertheless, the proximity of the latter with respect to the continental arc (Hervé et al., 2018) makes the presence of two adjacent subduction zones unlikely. Alternatively, the development of a Carboniferous advancing accretionary orogen might be a likely trigger for the Gondwanide orogeny (Fig. 9b), since it might increase the interplate coupling, thus leading to crustal thickening and a relative stabilization of the margin (e.g., Cawood et al., 2009). Therefore, the Gondwanide orogeny might be essentially linked to the evolution of a transpressional advancing orogen, developed along the continental margin of southwestern Gondwana.

5.3. The basement record of Mesozoic tectonomagmatic events

Monazite has a relatively high closure temperature for Pb diffusion, being >800 °C for grain sizes larger than 10 μm and cooling rates of 10 °C/my (Cherniak et al., 2004). Th diffusion is approximately three times slower than Pb diffusion (Cherniak & Pyle, 2008) and, therefore, the Th-U-Pb system should remain closed in monazite under low-grade metamorphic conditions. Nevertheless, monazite commonly records low-grade metamorphic and hydrothermal events (e.g., Poitrasson et al., 1996; Teufel & Heinrich, 1997; Just et al., 2010; Oyhantçabal et al., 2012; Bergemann et al., 2017). Such disturbances of the Th-U-Pb system seem to arise from mechanisms such as neocrystallization, recrystallization and dissolution/reprecipitation, instead from diffusive exchange (Cherniak et al., 2004; Gardés et al., 2006; Cherniak & Pyle, 2008; Kelsey et al., 2008; Harlov et al., 2011; Oriolo et al., 2018).

Though Jurassic magmatism is widespread in the North Patagonian Cordillera (Castro et al., 2011a; Echaurren et al., 2017), evidence of coeval metamorphism and associated deformation is still scarce. In the study area, the igneous-metamorphic basement hosts the Jurassic Cordilleran batholith, which yields U-Pb SHRIMP zircon crystallization ages of ca. 176-160 Ma (Castro et al., 2011a). The only Jurassic record reported so far for basement rocks is a EPMA Th-U-Pb monazite age of 169.6 ± 6.7 Ma for a micaschist of the Catedral hill, which was attributed to contact metamorphism caused by Jurassic magmatism (Martínez et al., 2012), possibly related to a close tonalitic intrusion. Interestingly, monazite data (Section 4.4) record comparable Middle Jurassic ages of 171 ± 9 and 170 ± 7 Ma. Microstructural evidence shows that Jurassic monazites are spatially associated with retrograde micas, which show shape-preferred orientation parallel to S_2 and are affected by F_3 microfolds and microkink bands (Figs. 5f, 7). Therefore, monazite ages are interpreted to record the timing of Jurassic low-grade metamorphism and deformation constrained at ca. 335 °C by chlorite thermometry. Though

Jurassic granitoids are absent in the Jurassic sample locations, the influence of magmatism in these ages cannot be discarded.

The here obtained monazite ages are similar to the U-Pb SHRIMP zircon age of 175.9 ± 4.9 Ma reported for a granulite xenolith enclosed in Paleogene basalts to the south of the North Patagonian Massif (Castro et al., 2011b), whereas slightly older Early Jurassic intraplate deformation was documented by K-Ar and Ar/Ar mica data of Paleozoic granitoids in the northeastern North Patagonian Massif (Martínez Dopico et al., 2017). Recently, extension-related very low-grade metamorphism was recognized in the Southern and Northern Neuquén Precordillera (Suárez & González, 2018). Further evidence suggesting a Jurassic age for low-grade metamorphism and deformation is provided by late deformation fabrics, so far considered to be related to the Gondwanide orogeny (García-Sansegundo et al., 2009). Sample BA 11-18 was collected close to conjugated kink bands (Fig. 4), which are also microscopically observed (Fig. 5f, Text S1 in the Supporting Information). Considering the orientation and kinematics of both sets of kink bands (e.g., Cobbold et al., 1971; Carreras et al., 2013), a NNW-SSE shortening direction (present coordinates) can be inferred, further supported by magmatic fabrics of Jurassic plutons (Castro et al., 2011a). Comparable sets of conjugated brittle structures related to Jurassic deformation were reported to the southeast in the Deseado Massif (Reimer et al., 1996; Japas et al., 2013). Likewise, Jurassic volcanism, ore deposits and sedimentation recorded elsewhere in Patagonia have been mostly attributed to NE-SW to ENE-WSW extension and NW-SE to NNW-SSE shortening (Pankhurst et al., 2000; Rapela et al., 2005; Silvestro & Zubiri, 2008; Giacosa et al., 2010; Páez et al., 2011; Naipauer et al., 2012; Japas et al., 2017; Bechis et al., 2014b; Navarrete et al., 2016, 2018).

Considering the NNW to NW convergence direction along the proto-Andean paleo-Pacific margin determined for the ca. 180-160 Ma period (Müller et al., 2016) and all aforementioned structural evidence, a regional strike-slip-dominated transtensional regime can

thus be inferred for Patagonia in the Jurassic (Fig. 10a; e.g., Giacosa et al., 2010; Castro et al., 2011a; Japas et al., 2013). In such a setting, both kink bands and F_3 open folds can be explained (Section 4.1, Fig. 10a; Fossen et al., 2013). Besides, the extensional component might favor the development of a thermal anomaly, leading to a relatively high geothermal gradient (Castro et al., 2011b; Suárez and González, 2018) that may explain the obtained monazite ages (Fig. 6b).

Cretaceous monazite ages of 110 ± 10 and 80 ± 20 Ma are associated with randomly oriented fine-grained aggregates of chlorite + white mica + opaque minerals ± epidote, which in some cases are located along microveins. In this context, monazite ages seem to record the timing of hydrothermal activity, possibly related to Cretaceous granitoids in the North Patagonian Cordillera suggested by K-Ar and Rb-Sr ages of ca. 120-80 Ma (González Díaz, 1982, and references therein).

On the other hand, dextral NE-SW- to NNE-SSW-striking subvertical S_3' shear zones are comparable in terms of orientation and kinematics to dextral NE-SW- to NNE-SSW-striking subvertical faults related to Andean Neogene transpression in the North Patagonian Cordillera (Diraison et al., 1998). However, deformation conditions estimated for shear zones (Sections 4.2, 5.1) indicate that they underwent deformation in a deeper crustal level than Neogene faults and, therefore, a more likely Cretaceous age is inferred for shear zones. This is further supported by middle Cretaceous deformation associated with ENE-NE shortening directions documented in northwestern Patagonia, where coeval tectonic activity along NNW-SSE- to NNE-SSW-striking thrusts was also reported (Orts et al., 2012; Echaurren et al., 2016, 2017; Gianni et al., 2018). Hence, shear zones might result from an early Andean Cretaceous dextral transpressional event (Fig. 10b), probably associated with coeval magmatism and hydrothermal events recorded by monazite ages, as the latter match the onset of Andean tectonics at ca. 100-95 Ma (Somoza and Zaffarana, 2008). Nevertheless, further geologic,

geochronologic and structural data are still necessary to assess the evolution of Cretaceous tectonomagmatic and hydrothermal processes.

6. Conclusions

Combined field structural data with *in situ* EPMA Th-U-Pb monazite, petrologic and microstructural data allow reconstructing the P-T-D-t path of the Gondwanide basement of the North Patagonian Cordillera. For samples from the Challhuaco hill, the timing of development of the metamorphic S_2 foliation and associated L_2 lineations and F_2 folds is constrained by monazite ages of 299 ± 8 and 302 ± 16 Ma during or shortly after peak metamorphic conditions of ca. 650 °C and 11 kbar, whereas S_1-F_1 fabrics might be related to prograde metamorphism developed prior to these peak conditions. Within this framework, the evolution from S_1-F_1 to S_2-F_2 seem to be the result of progressive transpressional deformation.

The prograde P-T path recorded by samples of the Challhuaco hill together with regional evidence suggests Late Paleozoic crustal thickening. Contemporaneous metamorphism and deformation recorded by metamorphic complexes of northwestern Patagonia (Argentina) and accretionary complexes exposed further west (Chile) point to a common evolution of both areas, most likely resulting from Carboniferous transpression due to advancing subduction. Instead of the result of collision of large continental blocks, the Gondwanide orogeny might thus be essentially linked to geodynamic processes associated with subduction along the proto-Pacific margin of Gondwana.

On the other hand, monazite ages of 171 ± 9 and 170 ± 7 Ma indicate a Middle Jurassic low-grade metamorphic overprint coeval with development of kink bands and F_3 open folds. This Middle Jurassic deformation event was contemporaneous with the emplacement of Cordilleran granitoids in the North Patagonian Cordillera and might result from a regional

transtensional event, ubiquitously recorded in Patagonia. Finally, monazite ages of 110 ± 10 and 80 ± 20 Ma are interpreted to result from hydrothermal processes, possibly related to Cretaceous magmatism. The timing of deformation along low-grade dextral NE-SW- to NNE-SSW-striking subvertical shear zones seems to be coeval, thus recording middle Cretaceous dextral transpression associated with the onset of Andean tectonics.

Acknowledgements

Sebastián Oriolo thanks financial support of the National Geographic Society (grant CP-123R-17) and Agencia Nacional de Promoción Científica y Tecnológica (PICT-2017-1092). Support at the SEM studies in the Laboratory of Geometallurgy at Freiberg was provided by S. Gilbricht. Pablo González thanks financial support of the Universidad Nacional de Río Negro (PI-UNRN-40-A-462) and Agencia Nacional de Promoción Científica y Tecnológica (PICT-2015-0787), whereas Florencia Bechis acknowledges financial support of the Agencia Nacional de Promoción Científica y Tecnológica (PICT-2010-2240 and PICT-2017-3259). The authors also wish to thank the administration of the Parque Nacional Nahuel Huapi for allowing field work in the area. Mariano Sebesta and all people from the Refugio Agostino Rocca and Refugio López are greatly acknowledged for their hospitality during the fieldwork. John Geissman is thanked for the editorial handling and Djordje Grujic, Pedro Castiñeiras and Werner von Gosen for their critical comments, which significantly contributed to improve the manuscript. All data used in the manuscript are available in the text, figures and Supporting Information (Text S1 and S2, Tables S1 and S2). In the case of previously published data, data are referred to their source, which are listed in the References.

References

Bechis, F., Encinas, A., Concheyro, A., Litvak, V. D., Aguirre-Urreta, B., & Ramos, V. A. (2014a). New age constraints for the Cenozoic marine transgressions of northwestern Patagonia, Argentina (41°-43° S): Paleogeographic and tectonic implications. *Journal of South American Earth Sciences*, *52*, 72-93.

Bechis, F., Cristallini, E. O., Giambiagi, L. B., Yagupsky, D. L., Guzmán, C. G., & García, V. H. (2014b). Transtensional tectonics induced by oblique reactivation of previous lithospheric anisotropies during the Late Triassic to Early Jurassic rifting in the Neuquén basin: Insights from analog models. *Journal of Geodynamics*, *79*, 1-17.

Bernet, M. (2009). A field-based estimate of the zircon fission-track closure temperature. *Chemical Geology*, *259*, 181-189.

Bergemann, C., Gnos, E., Berger, A., Whitehouse, M., Mullis, J., Wehrens, P., Pettke, T., & Janots, E. (2017) Th- Pb ion probe dating of zoned hydrothermal monazite and its implications for repeated shear zone activity: An example from the Central Alps, Switzerland. *Tectonics*, *36*, 671-689.

Bosse, V., & Villa, I. M. (2019). Petrochronology, hygrochronology of tectono-metamorphic events. Gondwana Research. https://doi.org/10.1016/j.gr.2018.12.014

Carreras, J., & Druguet, E. (2018). Complex fold patterns developed by progressive deformation. *Journal of Structural Geology*. https://doi.org/10.1016/j.jsg.2018.07.015

Carreras, J., Cosgrove, J. W., & Druguet, E. (2013). Strain partitioning in banded and/or anisotropic rocks: Implications for inferring tectonic regimes. *Journal of Structural Geology*, *50*, 7-21.

Castillo, P., Fanning, C. M., Pankhurst, R. J., Hervé, F., & Rapela, C. W. (2017). Zircon O- and Hf-isotope constraints on the genesis and tectonic significance of Permian magmatism in Patagonia. *Journal of the Geological Society*, *174*, 803-816.

Castro, A., Moreno-Ventas, I., Fernández, C., Vujovich, G., Gallastegui, G., Heredia, N., Martino, R. D., Becchio, R., Corretgé, L. G., Díaz-Alvarado, J., Such, P., García-Arias, M., & Liu, D. -Y. (2011a). Petrology and SHRIMP U-Pb zircon geochronology of Cordilleran granitoids of the Bariloche area, Argentina. *Journal of South American Earth Sciences*, *32*, 508-530.

Castro, A., Aragón, E., Díaz-Alvarado, J., Blanco, I., García-Casco, A., Vogt, K., & Liu, D. -Y. (2011b). Age and composition of granulite xenoliths from Paso de Indios, Chubut province, Argentina. *Journal of South American Earth Sciences*, *32*, 567-574.

Cerredo, M. E., & López de Luchi, M. G. (1998). Mamil Choique Granitoids, southwestern North Patagonian Massif, Argentina: magmatism and metamorphism associated with a polyphasic evolution. *Journal of South American Earth Sciences*, *11*, 499-515.

Chapman, J. B., Ducea, M. N., DeCelles, P. G., & Profeta, L. (2015). Tracking changes in crustal thickness during orogenic evolution with Sr/Y: An example from the North American Cordillera. *Geology*, *43*, 919-922.

Cherniak, D. J., & Pyle, J. M. (2008). Th diffusion in monazite. *Chemical Geology*, *256*, 52-61.

Cherniak, D. J., Watson, E. B., Grove, M., & Harrison, T. M. (2004). Pb diffusion in monazite: A combined RBS/SIMS study. *Geochimica et Cosmochimica Acta*, *68*, 829-840.

Chiaradia, M. (2015). Crustal thickness control on Sr/Y signatures of recent arc magmas: an Earth scale perspective. *Scientific Reports*, *5*, 8115.

Cingolani, C. A., Zanettini, J. C. M., & Leanza, H. A. (2011). El basamento ígneo y metamórfico. In H. A. Leanza, C. Arregui, O. Carbone, J. C. Danieli, J. M. Vallés (Eds.), *Relatorio del XVIII Congreso Geológico Argentino* (pp. 37-47). Neuquén: Asociación Geológica Argentina.

Cobbold, P. R., Cosgrove, J. W., & Summers, J. M. (1971). Development of internal structures in deformed anisotropic rocks. *Tectonophysics*, *12*, 23-53.

Dalla Salda, L. H., Cingolani, C. A., & Varela, R. (1991). El basamento cristalino de la región norpatagónica de los lagos Gutiérrez, Mascardi y Guillelmo, provincia de Río Negro. *Revista de la Asociación Geológica Argentina*, *46*, 263-276.

Dalla Salda, L. H., Dalziel, I. W. D., Cingolani, C. A., & Varela, R. (1992). Did the Taconic Appalachians continue into southern South America? *Geology*, *20*, 1059-1062.

Diraison, M., Cobbold, P. R., Rossello, E. A., & Amos, A. J. (1998). Neogene dextral transpression due to oblique convergence across the Andes of northwestern Patagonia, Argentina. *Journal of South American Earth Sciences*, *11*, 519-532.

Duhart, P., McDonough, M., Muñoz, J., Martin, M., & Villeneuve, M. (2001). El Complejo Metamórfico Bahía Mansa en la cordillera de la Costa (39°30'-42°00'S): geocronología K-Ar, $^{40}Ar/^{39}Ar$ y U-Pb e implicancias en la evolución del margen sur-occidental de Gondwana. *Revista Geológica de Chile*, *28*, 179-208.

Echaurren, A., Folguera, A., Gianni, G., Orts, D., Tassara, A., Encinas, A., Giménez, M., & Valencia, V. (2016). Tectonic evolution of the North Patagonian Andes (41°–44° S) through recognition of syntectonic strata. *Tectonophysics*, *677-678*, 99-114.

Echaurren, A., Oliveros, V., Folguera, A., Ibarra, F., Creixell, C., & Lucassen, F. (2017). Early Andean tectonomagmatic stages in north Patagonia: insights from field and geochemical data. *Journal of the Geological Society*, *174*, 405-421.

Endo, S., & Wallis, S. R. (2017). Structural architecture and low- grade metamorphism of the Mikabu- Northern Chichibu accretionary wedge, SW Japan. *Journal of Metamorphic Geology*, *35*, 695-716.

Fagereng, Å., & Toy, V. G. (2011). Geology of the earthquake source: an introduction. In Å. Fagereng, V. G. Toy, J. V. Rowland (Eds.), Geology of the earthquake source: a volume in honour of Rick Sibson (Vol. 359, pp. 1-16). London: Geological Society of London.

Fossen, H., Teyssier, C., & Whitney, D. L. (2013). Transtensional folding. *Journal of Structural Geology*, *56*, 89-102.

Fossen, H., Cavalcante, G. C. G., Pinheiro, R. V. L., & Archanjo, C. J. (2018). Deformation – Progressive or multiphase? *Journal of Structural Geology.* https://doi.org/10.1016/j.jsg.2018.05.006

Franzese, J. R. (1993). *Deformación preandina del basamento del Cordón de la Piedra Santa, Neuquén*. Paper presented at the XII Congreso Geológico Argentina, Mendoza, Argentina.

Franzese, J. R. (1995). El Complejo Piedra Santa (Neuquén, Argentina): parte de un cinturón metamórfico neopaleozoico del Gondwana suroccidental. *Revista Geológica de Chile, 22*, 193-202.

García-Sansegundo, J., Farías, P., Gallastegui, G., Giacosa, R. E., & Heredia, N. (2009). Structure and metamorphism of the Gondwanan basement in the Bariloche region (North Patagonian Argentine Andes). *International Journal of Earth Sciences, 98*, 1599-1608.

Gardés, E., Jaoul, O., Montel, J. -M., Seydoux-Guillaume, A. -M., & Wirth, R. (2006). Pb diffusion in monazite: An experimental study of $Pb^{2+}+Th^{4+}\Leftrightarrow 2Nd^{3+}$ interdiffusion. *Geochimica et Cosmochimica Acta, 70*, 2325-2336.

Gasser, D., Jeřábek, P., Faber, C., Stünitz, H., Menegon, L., Corfu, F., Erambert, M., & Whitehouse, M. J. (2015). Behaviour of geochronometers and timing of metamorphic reactions during deformation at lower crustal conditions: phase equilibrium modelling and U-Pb dating of zircon, monazite, rutile and titanite from the Kalak Nappe Complex, northern Norway. *Journal of Metamorphic Geology*, *33*, 513-534.

Giacosa, R. E., & Heredia, N. (2004). Estructura de los Andes Nordpatagónicos en los cordones Piltriquitrón y Serrucho y en el valle de El Bolsón (41º 30´ - 42 º 00´ S), Río Negro. *Revista de la Asociación Geológica Argentina, 59*, 91-102.

Giacosa, R., Heredia, N., Césari, O., & Zubia, M. (2001). *Hoja 4172-IV, San Carlos de Bariloche (provincias de Río Negro y Bariloche)*. Buenos Aires: Instituto de Geología y Recursos Minerales (IGRM) – SEGEMAR.

Giacosa, R., Márquez, M., Nillni, A., Fernández, M., Fracchia, D., Parisi, C., Afonso, J., Paredes, J., & Sciutto, J. (2004). Litología y estructura del basamento ígneo-metamórfico del borde SO del Macizo Nordpatagónico al oeste del río Chico, (Cushamen, Chubut, 42º 10´S - 70º 30´O). *Revista de la Asociación Geológica Argentina*, *59*, 569-577.

Giacosa, R. E., Afonso, J., Heredia, N. C., & Paredes, J. (2005). Tertiary tectonics of the sub-Andean region of the North Patagonian Andes, southern central Andes of Argentina (41 - 42°30'S. *Journal of South American Earth Sciences*, *20*, 157-170.

Giacosa, R., Zubía, M., Sánchez, M., & Allard, J. (2010). Meso-Cenozoic tectonics of the southern Patagonian foreland: Structural evolution and implications for Au-Ag veins in the eastern Deseado Region (Santa Cruz, Argentina). *Journal of South American Earth Sciences*, *30*, 134-150.

Gianni, G. M., Dávila, F. M., Echaurren, A., Fennell, L., Tobal, J., Navarrete, C., Quezada, P., Folguera, A., & Giménez, M. (2018). A geodynamic model linking Cretaceous orogeny, arc migration, foreland dynamic subsidence and marine ingression in southern South America. *Earth-Science Reviews*, *185*, 437-462.

Goncalves, P., Oliot, E., Marquer, D., & Connolly, J. A. D. (2012). Role of chemical processes on shear zone formation: an example from the Grimsel metagranodiorite (Aar massif, Central Alps). *Journal of Metamorphic Geology*, *30*, 703-722.

González, P. D., Tortello, F., & Damborenea, S. (2011). Early Cambrian Archaeocyathan limestone blocks in low-grade metaconglomerate from El Jagüelito Formation (Sierra Grande, Río Negro, Argentina). *Geologica Acta*, *9*, 159-163.

González, P. D., Tortello, M., Damborenea, S., Naipauer, M., Sato, A. M., & Varela, R. (2012). Archaeocyaths from South America: review and new record. *Geological Journal*, *48*, 114-125.

González Bonorino, F. (2001). *Geología entre San Carlos de Bariloche y Llao Llao*. San Carlos de Bariloche: Fundación Bariloche.

González Díaz, E. F. (1982) Chronological zonation of granitic plutonism in the Northern Patagonian Andes of Argentina: the migration of intrusive cycles. *Earth-Science Reviews*, *18*, 365-393.

Goscombe, B. D., & Gray, D. R. (2009). Metamorphic response in orogens of different obliquity, scale and geometry. *Gondwana Research*, *15*, 151-167.

Greco, R. (2001). *Hoja 40a, Monte Tronador, provincia de Río Negro*. Buenos Aires: Servicio Geológico Nacional.

Gregori, D. A., Kostadinoff, J., Strazzere, L., & Raniolo, A. (2008). Tectonic significance and consequences of the Gondwanide orogeny in northern Patagonia, Argentina. *Gondwana Research*, *14*, 429-450.

Gregori, D. A., Saini-Eidukat, B., Benedini, L., Strazzere, L., Barros, M., & Kostadinoff, J. (2016). The Gondwana Orogeny in northern North Patagonian Massif: Evidences from the Caita Có granite, La Seña and Pangaré mylonites, Argentina. *Geoscience Frontiers*, *7*, 621-638.

Harlov, D. E., Wirth, R., & Hetherington, C. J. (2011). Fluid-mediated partial alteration of monazite: the role of coupled dissolution-reprecipitation during apparent solid state element mass transfer. *Contributions to Mineralogy and Petrology*, *162*, 329-348.

Heredia, N., García-Sansegundo, J., Gallastegui, G., Farías, P., Giacosa, R. E., Giambiagi, L. B., Busquets, P., Colombo, F., Charrier, R., Cuesta, A., Rubio-Ordónez, Á., & Ramos, V. A. (2017). Review of the geodynamic evolution of the SW margin of Gondwana preserved in the Central Andes of Argentina and Chile (28°-38° S latitude). *Journal of South American Earth Sciences*. https://doi.org/10.1016/j.jsames.2017.11.019

Heredia, N., García-Sansegundo, J., Gallastegui, G., Farias, P., Giacosa, R., Hongn, F., Tubía, J. M., Alonso, J. L., Busquets, P., Charrier, R., Clariana, P., Colombo, F., Cuesta, A., Gallastegui, J., Giambiagi, L., González-Menéndez, L., Limarino, C. O., Martín-Gonzalez, F., Pedreira, D., Quintana, L., Rodríguez-Fernández, L. R., Rubio-Ordoñez, A., Seggiaro, R. E., Serra-Varela, S., Spalletti, L., Cardó, R., & Ramos, V. A. (2018). The Pre-Andean phases of construction of the Southern Andes basement in Neoproterozoic-Paleozoic times. In A. Folguera, E. Contreras Reyes, N. Heredia, A. Encinas, S. Iannelli, V. Oliveros, F. Dávila, G. Collo, L. Giambiagi, A. Maksymowicz, P. Iglesia Llanos, M. Turienzo, M. Naipauer, D. M.

Orts, V. Litvak, O. Alvarez, C. Arriagada (Eds.), *The Evolution of the Chilean-Argentinean Andes* (pp. 133-153). Cham: Springer International Publishing AG.

Hervé, F., Haller, M. J., Duhart, P., & Fanning, C. M. (2005). *SHRIMP U-Pb ages of detrital zircons from Cushamen and Esquel formations, North Patagonian Massif, Argentina: Geological implications*. Paper presented at the XVI Congreso Geológico Argentino, La Plata, Argentina.

Hervé, F., Calderón, M., Fanning, C. M., Pankhurst, R. J., & Godoy, E. (2013). Provenance variations in the Late Paleozoic accretionary complex of central Chile as indicated by detrital zircons. *Gondwana Research*, *23*, 1122-1135.

Hervé, F., Calderon, M., Fanning, C. M., Pankhurst, R. J., Fuentes, F., Rapela, C. W., Correa, J., Quezada, P., & Marambio, C. (2016). Devonian magmatism in the accretionary complex of southern Chile. *Journal of the Geological Society*, *173*, 587-602.

Hervé, F., Calderon, M., Fanning, C. M., Pankhurst, R. J., Rapela, C. W., & Quezada, P. (2018). The country rocks of Devonian magmatism in the North Patagonian Massif and Chaitenia. *Andean Geology*, *45*, 301-317.

Hobbs, B. E., Ord, A., & Regenauer-Lieb, K. (2011). The thermodynamics of deformed metamorphic rocks: A review. *Journal of Structural Geology*, *33*, 758-818.

Holdaway, M. J. (2000). Application of new experimental and garnet Margules data to the garnet-biotite geothermometer. *American Mineralogist*, *85*, 881-892.

Horton, B. K. (2018). Sedimentary record of Andean mountain building. *Earth-Science Reviews*, *178*, 279-309.

Iannelli, S. B., Litvak, V. D., Fernández Paz, L., Folguera, A., Ramos, M. E., & Ramos, V. A. (2017). Evolution of Eocene to Oligocene arc-related volcanism in the North Patagonian Andes (39-41°S), prior to the break-up of the Farallon plate. *Tectonophysics*, *696-697*, 70-87.

Janots, E., Brunet, F., Goffé, B., Poinssot, C., Burchard, M., & Cemic, L. (2007). Thermochemistry of monazite-(La) and dissakisite-(La): implications for monazite and allanite stability in metapelites. *Contributions to Mineralogy and Petrology*, *154*, 1-14.

Japas, M. S., Sruoga, P., Kleiman, L. E., Gayone, M. R., Maloberti, A., & Comito, O. (2013). Cinemática de la extensión jurásica vinculada a la provincia silícea Chon Aike, Santa Cruz, Argentina. *Revista de la Asociación Geológica Argentina*, *70*, 16-30.

Japas, M. S., Vizán, H., Prezzi, C., Geune, S. E., Franzese, J., Renda, E., & Oriolo, S. (2017). *Pangea, autosubducción y cuencas extensionales mesozoicas del margen sudoeste de Gondwana*. Paper presented at the XX Congreso Geológico Argentina, San Miguel de Tucumán, Argentina.

Johnson, S. E. (1999). Porphyroblast microstructures: A review of current and future trends. *American Mineralogist*, *84*, 1711-1726.

Jones, R. R., Holdsworth, R. E., Clegg, P., Tavarnelli, E., & McCaffrey, K. J. W. (2004). Inclined Transpression. *Journal of Structural Geology*, *26*, 1531-1548.

Just, J., Schulz, B., de Wall, H., Jourdan, F., & Pandit, M. K. (2010). Monazite CHIME/EPMA dating of Erinpura granitoid deformation: implications for Neoproterozoic tectono-thermal evolution of NW India. *Gondwana Research*, *19*, 402-412.

Kato, T. T., Sharp, W., & Godoy, E. (2008). Inception of a Devonian subduction zone along the southwestern Gondwana margin: $^{40}Ar/^{39}Ar$ dating of eclogite-amphibolite assemblage in blueschist boulders from the coastal range of Chile (41°S). *Canadian Journal of Earth Sciences*, *45*, 337-351.

Keidel, H. (1938). Über die "Gondwaniden" Argentiniens. *Geologische Rundschau*, *30*, 148-240.

Kelsey, D. E., Clark, C., & Hand, M. (2008). Thermobarometric modelling of zircon and monazite growth in melt- bearing systems: Examples using model metapelitic and metapsammitic granulites. *Journal of Metamorphic Geology*, *26*, 199-212.

López de Luchi, M. G., & Cerredo, M. E. (2010). Geochemistry of the Mamil Choique granitoids at Río Chico, Río Negro, Argentina: Late Paleozoic crustal melting in the North Patagonian Massif. *Journal of South American Earth Sciences*, *25*, 526-546.

Ludwig, K. R. (2001). User manual for Isoplot/Ex (rev. 2.49): a geochronological toolkit for Microsoft Excel. Berkeley: Berkeley Geochronology Center Special Publication.

Marcos, P., Gregori, D. A., Benedini, L., Barros, M., Strazzere, L., & Pavón Pivetta, C. (2018). Pennsylvanian glacimarine sedimentation in the Cushamen Formation, western North Patagonian Massif. *Geoscience Frontiers*, *9*, 485-504.

Marsh, J. H., Johnson, S. E., Yates, M. G., & West Jr., D. P. (2009). Coupling of deformation and reactions during mid- crustal shear zone development: an *in situ* frictional-viscous transition. *Journal of Metamorphic Geology*, *27*, 531-553.

Martin, M. W., Kato, T. T., Rodríguez, C., Godoy, E., Duhart, P., McDonough, M., & Campos, A. (1999). Evolution of the late Paleozoic accretionary complex and overlying forearc-magmatic arc, south central Chile (38°-41°S): Constraints for the tectonic setting along the southwestern margin of Gondwana. *Tectonics*, *18*, 582-605.

Martínez, J. C., Dristas, J. A., & Massonne, H. -J. (2012). Palaeozoic accretion of the microcontinent Chilenia, North Patagonian Andes: high-pressure metamorphism and subsequent thermal relaxation. *International Geology Review*, *54*, 472-490.

Martínez Dopico, C. I., Tohver, E., López de Luchi, M. G., Wemmer, K., Rapalini, A. E., & Cawood, P. A. (2017). Jurassic cooling ages in Paleozoic to early Mesozoic granitoids of northeastern Patagonia: $^{40}Ar/^{39}Ar$, ^{40}K-^{40}Ar mica and U-Pb zircon evidence. *International Journal of Earth Sciences*, *106*, 2343-2357.

Montel, J. M., Foret, S., Veschambre, M., Nicollet, C., & Provost, A. (1996). Electron microprobe dating of monazite. *Chemical Geology*, *131*, 37-53.

Müller, R. D., Seton, M., Zahirovic, S., Williams, S. E., Matthews, K. J., Wright, N. M., Shephard, G. E., Maloney, K. T., Barnett-Moore, N., Hosseinpour, M., Bower, D. J., & Cannon, J. (2016). Ocean basin evolution and global-scale plate reorganization events since Pangea breakup. *Annual Review of Earth and Planetary Sciences*, *44*, 107-138.

Mulch, A., & Cosca, M. A. (2004). Recrystallization or cooling ages: in situ UV-laser $^{40}Ar/^{39}Ar$ geochronology of muscovite in mylonitic rocks. *Journal of the Geological Society, 161*, 573-582.

Naipauer, M., García Morabito, E., Marques, J. C., Tunik, M., Rojas Vera, E. A., Vujovich, G. I., Pimentel, M. P., & Ramos, V. A. (2012). Intraplate Late Jurassic deformation and exhumation in western central Argentina: Constraints from surface data and U-Pb detrital zircon ages. *Tectonophysics, 524-525*, 59-75.

Navarrete, C., Gianni, G., Echaurren, A., Lince Klinger, F., & Folguera, A. (2016). Episodic Jurassic to Lower Cretaceous intraplate compression in Central Patagonia during Gondwana breakup. *Journal of Geodynamics, 102*, 185-201.

Navarrete, C. R., Gianni, G., Echaurren, A., & Folguera, A. (2018). Lower Jurassic to Early Paleogene intraplate contraction in Central Patagonia. In A. Folguera, E. Contreras Reyes, N. Heredia, A. Encinas, S. Iannelli, V. Oliveros, F. Dávila, G. Collo, L. Giambiagi, A. Maksymowicz, P. Iglesia Llanos, M. Turienzo, M. Naipauer, D. M. Orts, V. Litvak, O. Alvarez, C. Arriagada (Eds.), *The Evolution of the Chilean-Argentinean Andes* (pp. 245-271). Cham: Springer International Publishing AG.

Oriolo, S., Oyhantçabal, P., Wemmer, K., Basei, M. A. S., Benowitz, J., Pfänder, J., Hannich, F., & Siegesmund, S. (2016a). Timing of deformation in the Sarandí del Yí Shear Zone, Uruguay: implications for the amalgamation of Western Gondwana during the Neoproterozoic Brasiliano-Pan-African Orogeny. *Tectonics, 35*, 754-771.

Oriolo, S., Oyhantçabal, P., Wemmer, K., Heidelbach, F., Pfänder, J., Basei, M. A. S., Hueck, M., Hannich, F., Sperner, B., & Siegesmund, S. (2016b). Shear zone evolution and timing of deformation in the Neoproterozoic transpressional Dom Feliciano Belt, Uruguay. *Journal of Structural Geology, 92*, 59-78.

Oriolo, S., Wemmer, K., Oyhantçabal, P., Fossen, H., Schulz, B., Siegesmund, S., 2018. Geochronology of shear zones – A review. *Earth-Science Reviews, 185*, 665-683. https://doi.org/10.1016/j.earscirev.2018.07.007

Orts, D. L., Folguera, A., Encinas, A., Ramos, M., Tobal, J., & Ramos, V. A. (2012). Tectonic development of the North Patagonian Andes and their related Miocene foreland basin (41°30′-43°S). *Tectonics, 31*, TC3012.

Oyhantçabal, P., Wegner-Eimer, M., Wemmer, K., Schulz, B., Frei, R., & Siegesmund, S. (2012). Paleo- and Neoproterozoic magmatic and tectonometamorphic evolution of the Isla Cristalina de Rivera (Nico Pérez Terrane, Uruguay). *International Journal of Earth Sciences, 101*, 1745-1762.

Páez, G. N., Ruiz, R., Guido, D. M., Jovic, S. M., & Schalamuk, I. B. (2011). Structurally controlled fluid flow: High-grade silver ore-shoots at Martha epithermal mine, Deseado Massif, Argentina. *Journal of Structural Geology, 33*, 985-999.

Pankhurst, R. J., Riley, T. R., Fanning, C. M., & Kelley, S. P. (2000). Episodic silicic volcanism in Patagonia and the Antarctic Peninsula: Chronology of magmatism associated with the break-up of Gondwana. *Journal of Petrology, 41*, 605-625.

Pankhurst, R. J., Rapela, C. W., Fanning, C. M., & Márquez, M. (2006). Gondwanide continental collision and the origin of the Patagonia. *Earth-Science Reviews*, *76*, 235-257.

Pankhurst, R. J., Rapela, C. W., López de Luchi, M. G., Rapalini, A. E., Fanning, C. M., & Galindo, C. (2014). The Gondwana connections of northern Patagonia. *Journal of the Geological Society*, *171*, 313-328.

Poitrasson, F., Chenery, S., & Bland, D. J. (1996). Contrasted monazite hydrothermal alteration mechanisms and their geochemical implications. *Earth and Planetary Science Letters*, *145*, 79-96.

Powell, R., & Holland, T. J. B. (1994). Optimal geothermometry and geobarometry. *American Mineralogist*, *79*, 120-133.

Powell, R., & Holland, T. J. B. (2008). On thermobarometry. *Journal of Metamorphic Geology*, *26*, 155-179.

Prezzi, C., Vizán, H., Renda, E., Vázquez, S., Oriolo, S., & Japas, M. S. (2018). Evolution of the Paleozoic Claromecó Basin (Argentina) and geodynamic implications for the southwestern margin of Gondwana: Insights from isostatic, gravimetric and magnetometric models. *Tectonophysics*, *742-743*, 120-136.

Profeta, L., Ducea, M. N., Chapman, J. B., Paterson, S. R., Henriquez Gonzales, S. M., Kirsch, M., Petrescu, L., & DeCelles, P. G. (2015). Quantifying crustal thickness over time in magmatic arcs. *Scientific Reports*, *5*, 17786.

Pyle, J. M., Spear, F. S., Rudnick, R. L., & McDonough, W. F. (2001). Monazite-xenotime-garnet equilibrium in metapelites and a new monazite-garnet thermometer. *Journal of Petrology*, *42*, 2083-2107.

Ponce, C., Druguet, E., & Carreras, J. (2013). Development of shear zone-related lozenges in foliated rocks. *Journal of Structural Geology*, *50*, 176-186.

Raimondo, T., Collins, A. S., Hand, M., Walker-Hallam, A., Hugh Smithies, R., Evins, P. M., & Howard, H. M. (2010). The anatomy of a deep intracontinental orogen. *Tectonics*, *29*, TC4024.

Ramos, V. A. (1984). *Patagonia: ¿Un continente paleozoico a la deriva?* Paper presented at IX Congreso Geológico Argentino, San Carlos de Bariloche, Argentina.

Ramos, V. A. (2008). Patagonia: A paleozoic continent adrift? *Journal of South American Earth Sciences*, *26*, 235-251.

Ramos, V. A., & Naipauer, M. (2014). Patagonia: where does it come from? *Journal of Iberian Geology*, *40*, 367-379.

Ramos, V.A., Folguera, A., García Morabito, E., 2011. Las provincias geológicas del Neuquén. In H. A. Leanza, C. Arregui, O. Carbone, J. C. Danieli, J. M. Vallés (Eds.), *Relatorio del XVIII Congreso Geológico Argentino* (pp. 317-326). Neuquén: Asociación Geológica Argentina.

Rapalini, A. E., López de Luchi, M., Martínez Dopico, C., Lince Klinger, F., Giménez, M., & Martínez, P. (2010). Did Patagonia collide with Gondwana in the Late Paleozoic? Some

insights from a multidisciplinary study of magmatic units of the North Patagonian Massif. *Geologica Acta*, *8*, 349-371.

Rapalini, A. E., López de Luchi, M., Tohver, E., & Cawood, P. A. (2013). The South American ancestry of the North Patagonian Massif: geochronological evidence for an autochthonous origin? *Terra Nova*, *25*, 337-342.

Rapela, C. W., Spalletti, L. A., Merodio, J. C., & Aragón, E. (1988). Temporal evolution and spatial variation of early Tertiary volcanism in the Patagonian Andes (40°S - 42°30'S). *Journal of South American Earth Sciences*, *1*, 75-88.

Rapela, C. W., Pankhurst, R. J., Fanning, C. M., & Hervé, F. (2005). Pacific subduction coeval with the Karoo mantle plume: the Early Jurassic Subcordilleran belt of northwestern Patagonia. In A. R. M. Vaughan, P. Y. Leat, R. J. Pankhurst (Eds.), *Terrane processes at the margins of Gondwana* (Vol. 246, pp. 217-239). London: Geological Society of London.

Reimer, W., Miller, H., & Mehl, H. (1996). Mesozoic and Cenozoic palaeo-stress fields of the South Patagonian Massif deduced from structural and remote sensing data. In B. C. Storey, E. C. King, R. A. Livermore (Eds.), *Weddell Sea tectonics and Gondwana break-up* (Vol. 108, pp. 73-85). London: Geological Society of London.

Renda, E., Oriolo, S. & Vizán, H. (2017). *Comparación estructural entre dos unidades de la Formación Mamil Choique: granitoide de Sierra del Medio (~253 Ma) y granodiorita Paso del Sapo (~314 Ma)*. Paper presented at the XX Congreso Geológico Argentina, San Miguel de Tucumán, Argentina.

Schulz, B. (2017). Polymetamorphism in garnet micaschists of the Saualpe Eclogite Unit (Eastern Alps, Austria), resolved by automated SEM methods and EMP-Th-U-Pb monazite dating. *Journal of Metamorphic Geology*, *35*, 141-163.

Serra-Varela, S., González, P. D., Giacosa, R. E., Heredia, N., & Sato, A. M. (2017). *Condiciones físicas del metamorfismo de alta temperatura y baja presión del basamento paleozoico inferior en el área de San Martín de los Andes, Neuquén*. Paper presented at XX Congreso Geológico Argentino, Córdoba, Argentina.

Serra-Varela, S., González, P. D., Giacosa, R. E., Heredia, N., Pedreira, D., Martín-González, F., & Sato, A. M. (2018). The poly-orogenic Palaeozoic basement of the Northpatagonian Andes in the San Martín de los Andes area (Neuquén, Argentina): Characteristics, age and correlations. *Andean Geology*. http://dx.doi.org/10.5027/andgeoV46n1-3124

Skrzypek, E., Schulmann, K., Štípská, P., Chopin, F., Lehmann, J., Lexa, O., & Haloda, J. (2011). Tectono-metamorphic history recorded in garnet porphyroblasts: insights from thermodynamic modelling and electron backscatter diffraction analysis of inclusion trails. *Journal of Metamorphic Geology*, *29*, 473-496.

Somoza, R., & Zafaranna, C.B. (2008). Mid-Cretaceous polar standstill of South America, motion of the Atlantic hotspots and the birth of the Andean cordillera. *Earth and Planetary Science Letters*, *271*, 267-277.

Spear, F. S. (1993). *Metamorphic phase equilibria and pressure-temperature-time paths*. Washington: Mineralogical Society of America Monograph Series, Washington.

Spear, F. S. (2010). Monazite-allanite phase relations in metapelites. *Chemical Geology*, *279*, 55-62.

Suárez, R. J., & González, P. D. (2018). Caracterización geológica del metamorfismo diastatermal mesozoico en la Cuenca Neuquina y su relación con la anomalía térmica en el sinrift. *Revista de la Asociación Geológica Argentina*, *75*, 457-472.

Suzuki, K., Adachi, M., & Kajizuka, I. (1994). Electron microprobe observations of Pb diffusion in metamorphosed detrital monazites. *Earth and Planetary Science Letters*, *128*, 391-405.

Tchato, D. T., Schulz, B., & Nzenti, J. -P. (2009). Electron microprobe dating and thermobarometry of Neoproterozoic metamorphic events in the Kekem area, Central African Fold Belt of Cameroon. *Neues Jahrbuch für Mineralogie – Abhandlungen*, *186*, 95-109.

Teufel, S., & Heinrich, W. (1997). Partial resetting of the U-Pb isotope system in monazite through hydrothermal experiments: An SEM and U-Pb isotope study. *Chemical Geology*, *137*, 273-281.

Turner, J. C. M. (1965). Estratigrafía de Aluminé y adyacencias (provincia del Neuquén). *Revista de la Asociación Geológica Argentina*, *20*, 153-181.

Urraza, I. A., Grecco, L. E., Delpino, S. H., & Arrese, M. L. (2008). Determination of rock ages by chemical analysis of Th, U, Pb in the mineral monazite (Ce, La, Th, REE, U)PO_4 using EPMA. Paper presented at Annual General Meeting and Research Day, Halifax, Canada.

Urraza, I. A., Grecco, L. E., Delpino, S. H., Arrese, M. L., & Rapela, C. W. (2011). Petrología y estructura del Complejo ígneo-metamórfico Aluminé, provincia de Neuquén, Argentina. *Andean Geology*, *38*, 98-118.

Urraza, I., Delpino, S., & Grecco, L. (2015). Counterclockwise post-emplacement evolution of metatroctolites from Aluminé igneous-metamorphic Complex, Neuquén, Argentina. *Andean Geology*, *42*, 36-55.

Varela, R., Basei, M. A. S., Cingolani, C. A., Siga Jr, O., & Passarelli, C. R. (2005). El basamento cristalino de los Andes norpatagónicos en Argentina: geocronología e interpretación tectónica. *Revista Geológica de Chile*, *32*, 167-187.

Varela, R., Gregori, D. A., González, P. D., & Basei, M. A. S. (2015). Caracterización geoquímica del magmatismo de arco devónico y carbonífero-pérmico en el noroeste de Patagonia, Argentina. *Revista de la Asociación Geológica Argentina*, *72*, 419-432.

Villa, I. M., Bucher, S., Bousquet, R., Kleinhanns, I. C., & Schmid, S. M. (2014). Dating polygenetic metamorphic assemblages along a transect across the Western Alps. *Journal of Petrology*, *55*, 803-830.

Vizán, H., Prezzi, C., Japas, M. S., Van Zele, M. A., Geuna, S. E., & Renda, E. M. (2015). Tracción de losa en el margen boreal del Océano Paleotetis y deformación en el interior de Gondwana (incluyendo el cordón plegado de Ventana). *Revista de la Asociación Geológica Argentina*, *72*, 355-377.

Vizán, H., Prezzi, C. B., Geuna, S. E., Japas, M. S., Renda, E. M., Franzese, J., van Zele, M. A. (2017). Paleotethys slab pull, self-lubricated weak lithospheric zones, poloidal and toroidal plate motions, and Gondwana tectonics. *Geosphere*, *13*, 1541-1554.

von Gosen, W. (2003). Thrust tectonics in the North Patagonian Massif (Argentina): Implications for a Patagonia plate. *Tectonics*, *22*, 1005.

von Gosen, W. (2009). Stages of Late Palaeozoic deformation and intrusive activity in the western part of the North Patagonian Massif (southern Argentina) and their geotectonic implications. *Geological Magazine*, *146*, 48-71.

von Gosen, W., & Loske, W. (2004). Tectonic history of the Calcatapul Formation, Chubut province, Argentina, and the "Gastre fault system". *Journal of South American Earth Sciences*, *18*, 73-88.

Wallis, D., Lloyd, G. E., Phillips, R. J., Parsons, A. J., & Walshaw, R. D. (2015). Low effective fault strength due to frictional-viscous flow in phyllonites, Karakoram Fault Zone, NW India. *Journal of Structural Geology*, *77*, 45-61.

Wehrens, P., Berger, A., Peters, M., Spillmann, T., & Herwegh, M. (2016). Deformation at the frictional-viscous transition: Evidence for cycles of fluid-assisted embrittlement and ductile deformation in the granitoid crust. *Tectonophysics*, *693*, 66-84

Williams, M. L., & Jercinovic, M. J. (2012). Tectonic interpretation of metamorphic tectonites: integrating compositional mapping, microstructural analysis and *in situ* monazite dating. *Journal of Metamorphic Geology*, *30*, 739-752.

Willner, A. P., Glodny, J., Gerya, T. V., Godoy, E., & Massonne, H. -J. (2004). A counterclockwise *PTt* path of high-pressure/low-temperature rocks from the Coastal Cordillera accretionary complex of south-central Chile: constraints for the earliest stage of subduction mass flow. *Lithos*, *75*, 283-310.

Willner, A. P., Gerdes, A., Massonne, H. -J., Schmidt, A., Sudo, M., Thomson, S. N., & Vujovich, G. (2011). The geodynamics of collision of a microplate (Chilenia) in Devonian times deduced by the pressure-temperature-time evolution within part of a collisional belt (Guarguaraz Complex, W-Argentina). *Contributions to Mineralogy and Petrology*, *162*, 303-327.

Wu, C. M. (2015). Revised empirical garnet-biotite-muscovite-plagioclase geobarometer in metapelites. *Journal of Metamorphic Geology*, *33*, 167-176.

Yakymchuk, C., & Godin, L. (2012). Coupled role of deformation and metamorphism in the construction of inverted metamorphic sequences: an example from far- northwest Nepal. *Journal of Metamorphic Geology*, *30*, 513-535.

Zappettini, E. O., Chernicoff, C. J., Santos, J. O. S., Dalponte, M., Belousova, E., & McNaughton, N. (2012). Retrowedge-related Carboniferous units and coeval magmatism in the northwestern Neuquén province, Argentina. *International Journal of Earth Sciences*, *101*, 2083-2104.

Zaun, P. E., & Wagner, G. A. (1985). Fission-track stability in zircons under geological conditions. *Nuclear Tracks and Radiation Measurements*, *10*, 303-307.

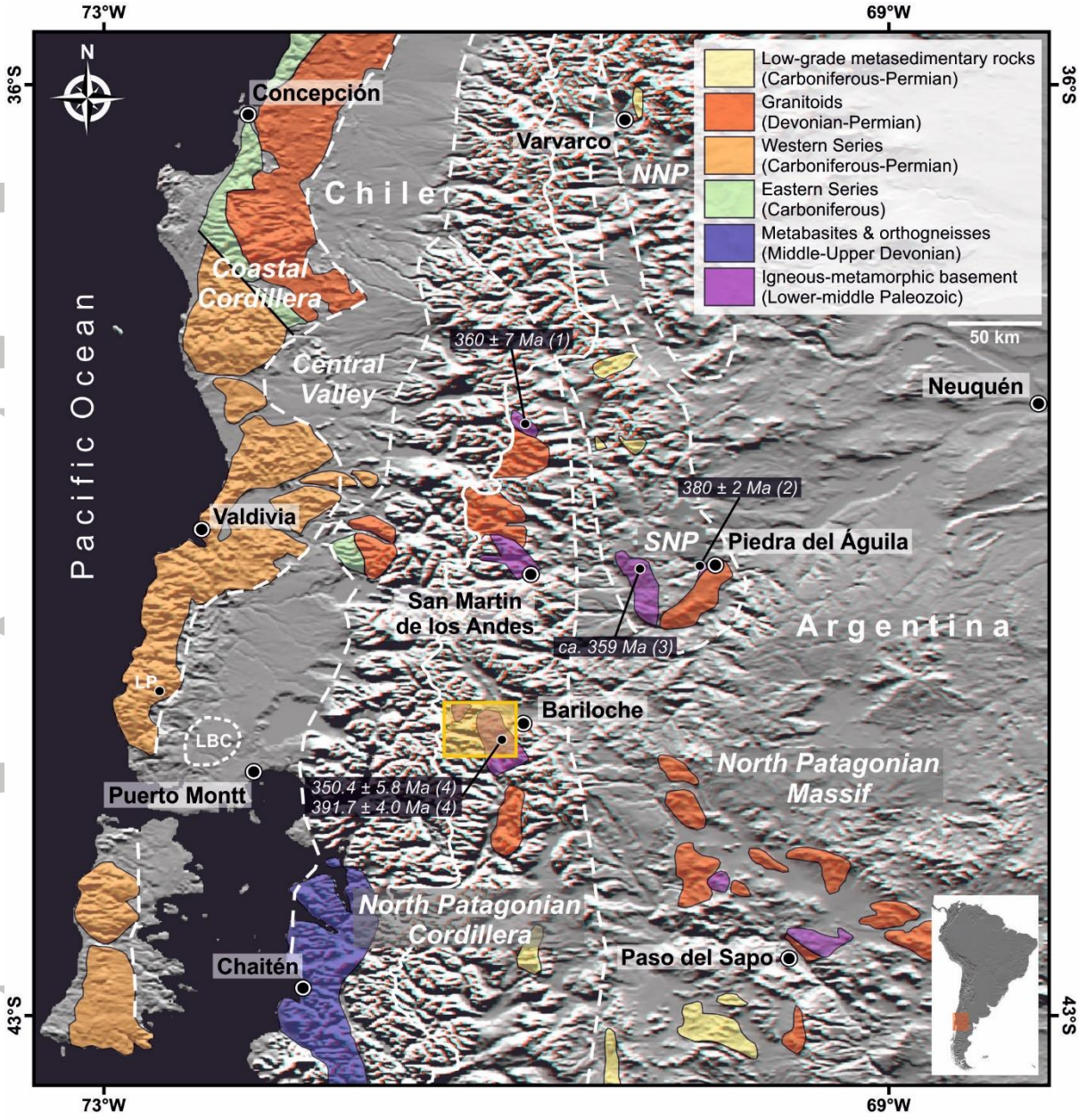

Fig. 1. Sketch map showing main exposures of Paleozoic basement rocks in northwestern Patagonia (modified after Cingolani et al., 2011; Hervé et al., 2011, 2013; Serra-Varela et al., 2018). Inset shows area of the map in South America, whereas the yellow rectangle indicates location of the map of Figure 2. Main morphostructural units are indicated with dotted white lines (modified after Ramos et al., 2011; Bechis et al., 2014): Coastal Cordillera, Central Valley, North Patagonian Cordillera, North Patagonian Massif, Southern Neuquén Precordillera (SNP) and Northern Neuquén Precordillera (NNP). Location of Los Pábilos boulders (LP) and borehole geochronologic data of the Llanquihue Basement Complex (LBC) is shown with dotted lines (Hervé et al., 2016). Geochronologic constraints on the timing of metamorphism of the metamorphic basement of Argentina are also indicated (1: EPMA Th-U-Pb monazite, Urraza et al., 2008; 2: U-Pb titanite, Lucassen et al., 2004; 3: U-Pb titanite, Varela et al., 2005; 4: EPMA Th-U-Pb monazite, Martínez et al., 2012).

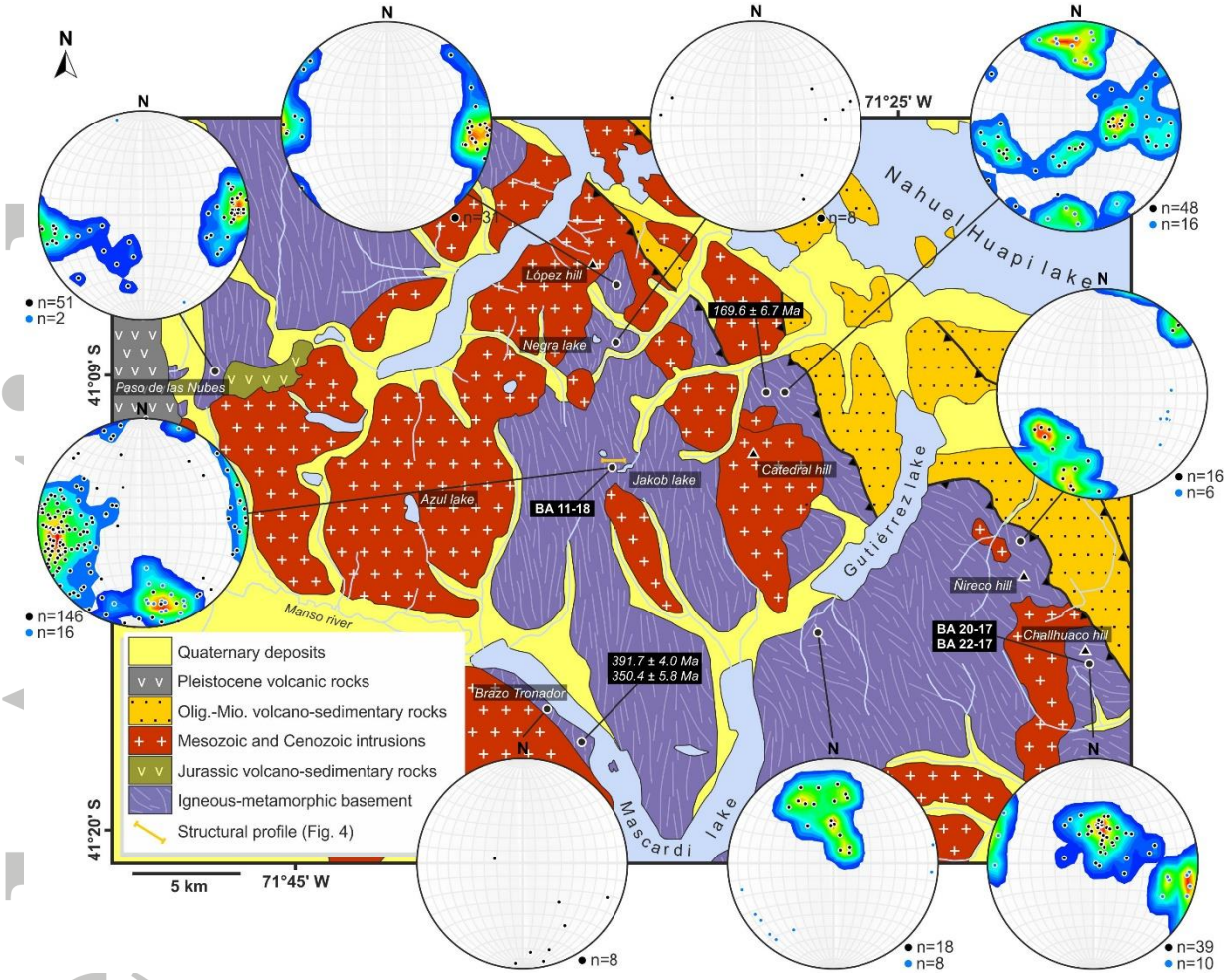

Fig. 2. Geologic map of the study area (modified after González Bonorino, 1973; Greco, 1975; García-Sansegundo et al., 2009; Bechis et al., 2014). Monazite geochronologic data (italics) of Martínez et al. (2012) and sample locations (bold) are shown. Lower hemisphere equal area projection of poles of S_2 (black dots) and L_2 (blue dots) are also presented. Contour intervals at 2 % per 1 % area.

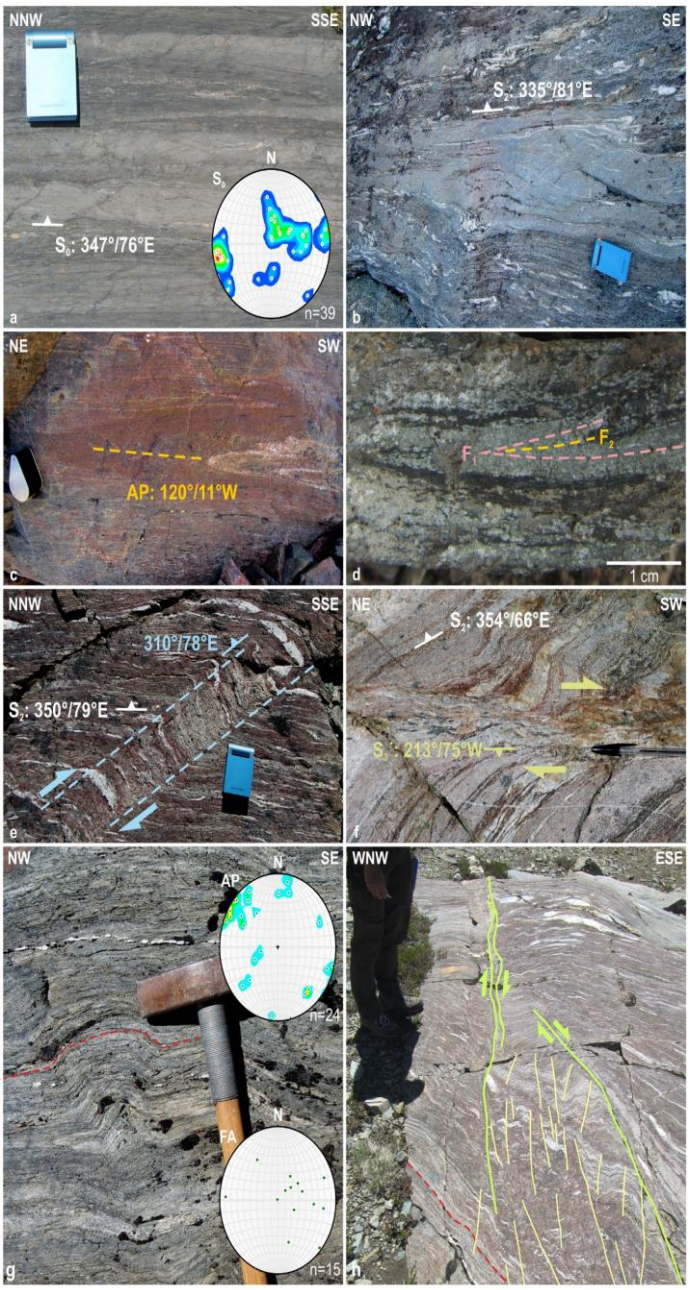

Fig. 3. (a) Bedding planes (S_0) defined by alternation of metapelites (dark grey) and metawackes (light grey). Lower hemisphere equal area projections of S_0 poles. Contour intervals at 2 % per 1 % area. (b) NNW-SSE-striking S_2 foliation in paragneisses. (c) Axial plane (AP) of isoclinal F_2 folds. (d) Axial plane traces of F_2 folds overprinting F_1 folds. (e) Dextral kink band cross-cutting S_2 planes. (f) Mylonitic S_3' foliation in a dextral shear zone. (g) Example of F_3 open kink fold. Lower hemisphere equal area projections of poles of F_3 axial planes (AP) and axes (FA). Contour intervals at 2 % per 1 % area. Red line shows the orientation of the S_2 foliation. (h) Development of crenulation cleavage (yellow lines) within a dextral shear zone lozenge, which corresponds to a contractional overstep (*sensu* Ponce et al., 2013). Red line shows the orientation of the S_2 foliation, whereas green lines indicate mylonitic S_3' foliation.

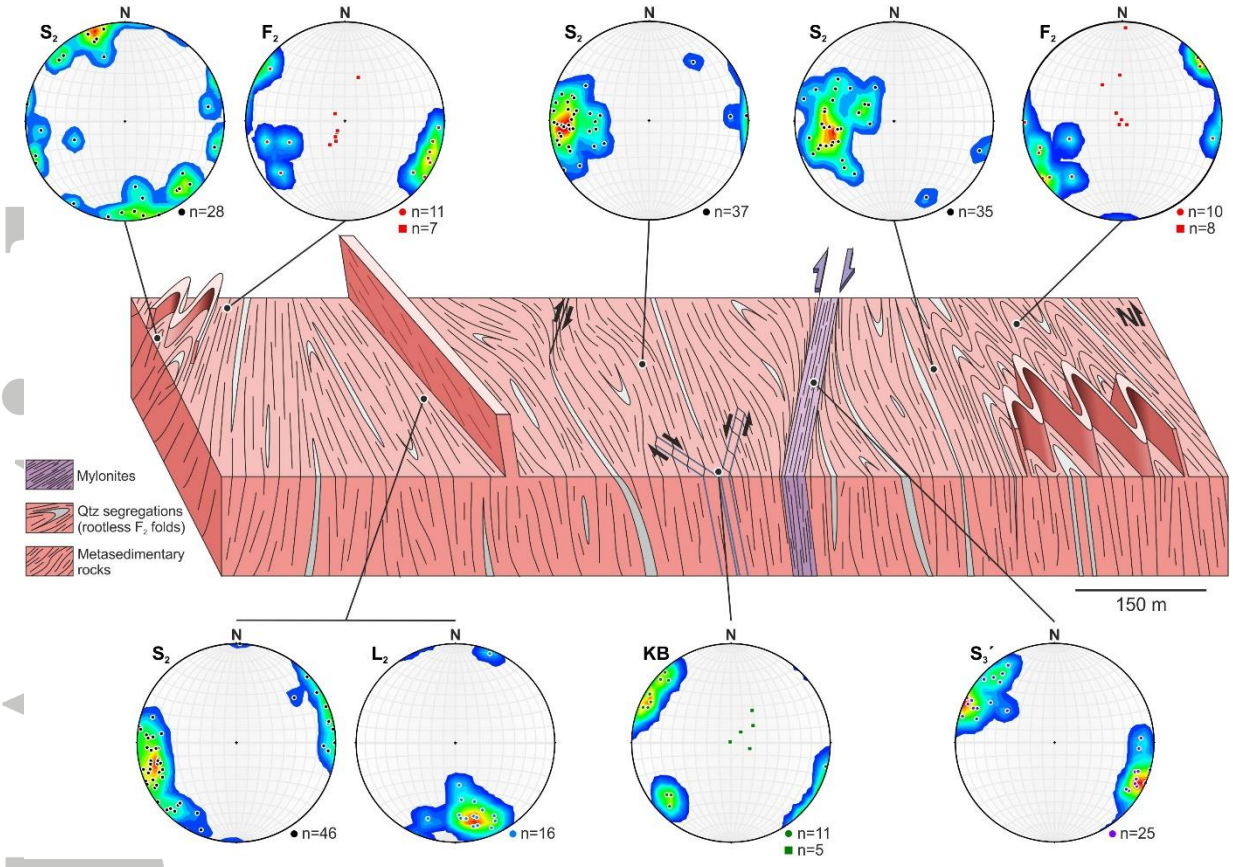

Fig. 4. Schematic structural profile at the western margin of the Jakob lake. Lower hemisphere equal area projections of poles of different structural elements are also shown. Contour intervals at 2 % per 1 % area. In the case of F_2 folds and kink bands (KB), circles and squares represent axial planes and axes, respectively. Rootless S_2 folds defined by quartz (Qtz) segregations are schematically illustrated.

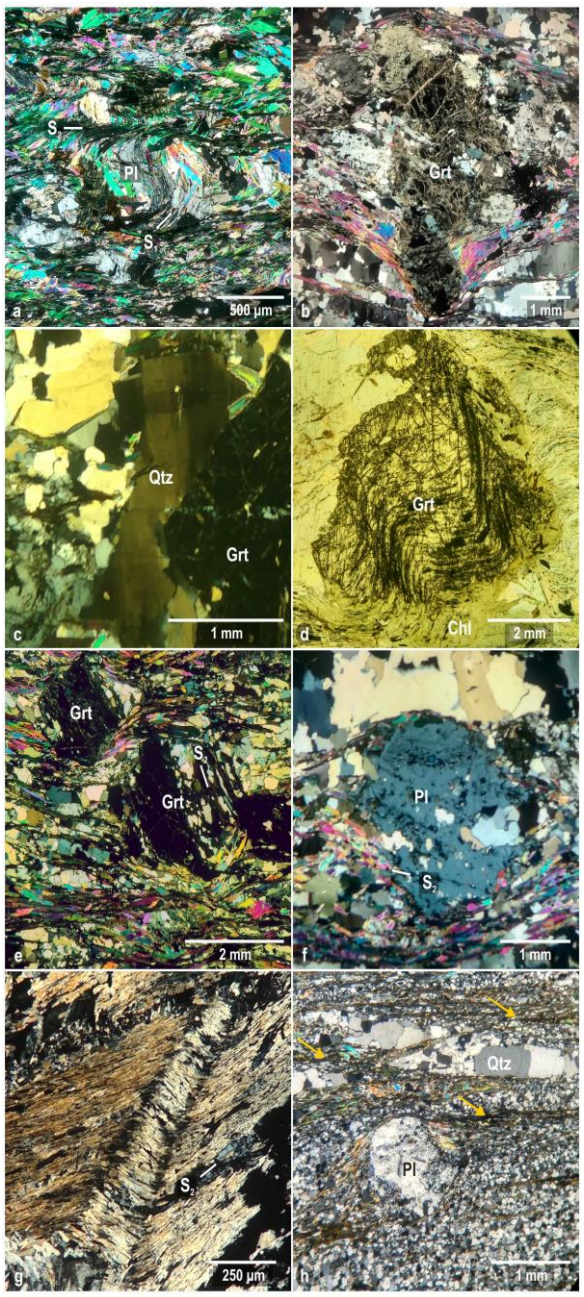

Fig. 5. Photomicrographs of gneisses and schists of the study area. (a) Crenulation of S_1 defined by inclusions of opaque minerals in plagioclase (Pl) and muscovite crystals (cross-polarized light). S_1 is preserved within microlithons of the S_2 crenulation schistosity. (b) Garnet (Grt) porphyroblast with S_2 strain shadows (cross-polarized light). (c) Chessboard extinction in quartz (cross-polarized light). (d) Relics of S_1 crenulation within a garnet porphyroblast, which show chlorite replacement along rims (plain-polarized light). (e) Relics of rotated S_2 foliation within garnet porphyroblasts (cross-polarized light). (f) Inclusion trails of opaque minerals within plagioclase porphyroblast that define an internal foliation, which is subparallel to S_2 in the matrix (cross-polarized light). (g) S_2 foliation replaced by retrograde white mica and chlorite and crosscut by microkink bands (cross-polarized light). (h) Ultramylonite showing plagioclase porphyroclast and monomineralic layers of granoblastic quartz in a fine-grained matrix (cross-polarized light). In the matrix, quartz is mostly granoblastic, whereas mica layers exhibit grain shape-preferred orientation and local concentration of opaque minerals in trails (yellow arrows) parallel to the mylonitic foliation.

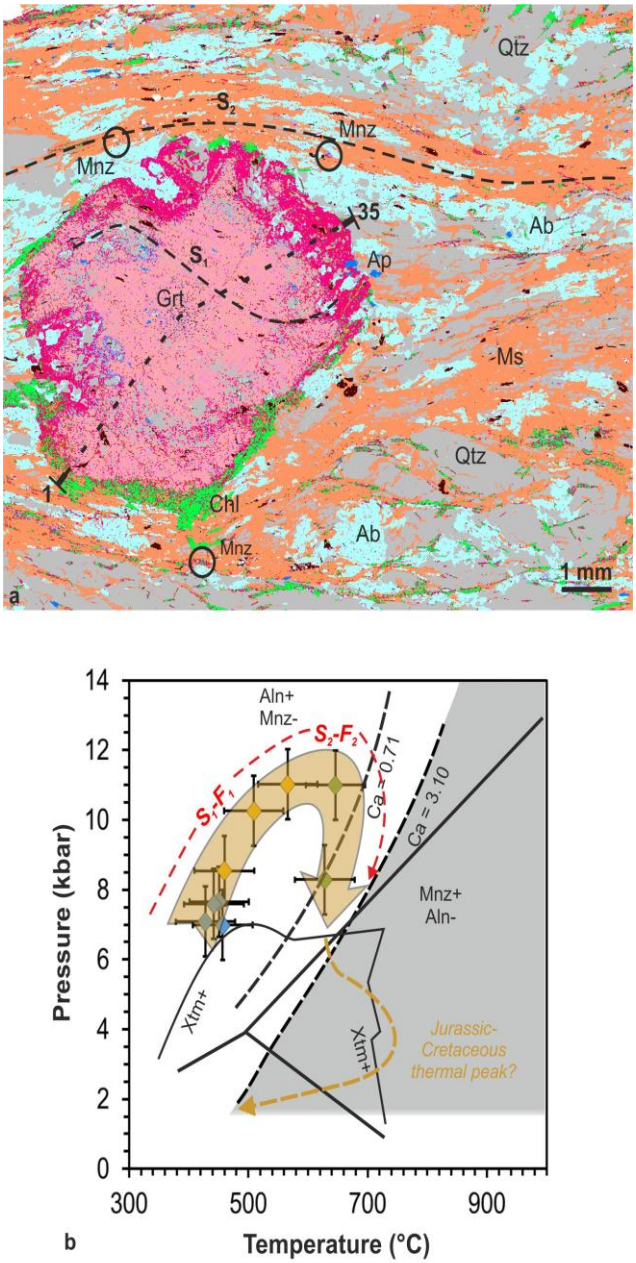

Fig. 6. (a) Map of energy dispersive X-ray (EDX) spectra (GXMAP) of sample BA 22-17 from the Challhuaco hill. Spectra from zoned garnet (Grt) with variable Fe, Mg, Mn and Ca contents in normalized element wt. % are labelled with different colors. EDX spectra from muscovite (Ms), albite (Ab), chlorite (Chl), quartz (Qtz) and apatite (Ap) are also indicated by distinct colors. Locations of analytical profile (1 to 35) and traces of garnet internal foliation S_1 and external foliation S_2 are marked as well. Positions of some monazites along S_2 are shown by circles. (b) P-T path of sample BA 22-17. Pressure estimations were obtained with the garnet-biotite-muscovite-plagioclase barometer (Wu, 2015), whereas temperature was calculated using garnet-biotite thermometer (Holdaway, 2000). Colors indicate garnet zonation (blue: core, yellow: middle, green: rim). Stability fields of monazite and allanite at different bulk rock contents as a function of Ca molar content (dotted lines) are shown together with the xenotime stability field (Janots et al., 2007; Spear, 2010). Stability fields of Al_2SiO_5 polymorphs are included as well. Mnz: monazite, Aln: allanite, Xtm: xenotime. Red arrows indicate the evolution of Carboniferous S_1-F_1 to S_2-F_2 fabrics related to the P-T path, whereas the brown arrow shows a schematic trajectory to explain Jurassic and Cretaceous monazite growth.

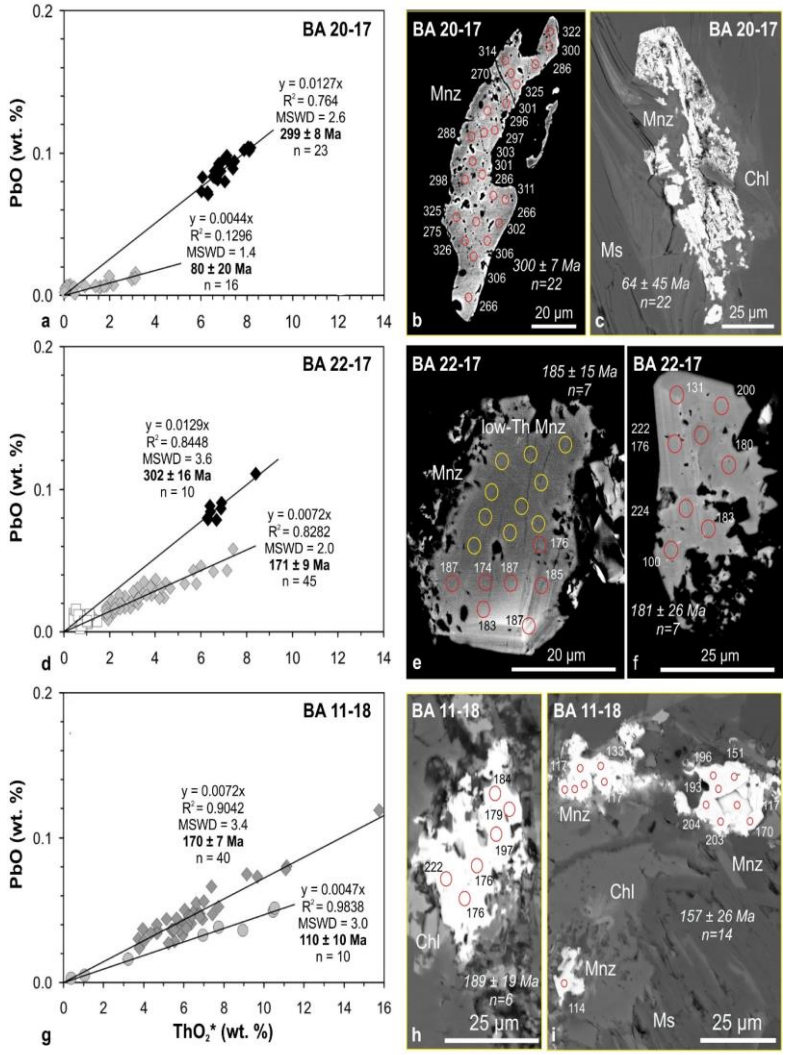

Fig. 7. Th-U-Pb chemical model ages of monazite (a, d, g). Total ThO_2* vs PbO (wt. %) isochrones diagrams. ThO2* is ThO_2 + UO_2 equivalents expressed as ThO_2. Regression lines with the coefficient of determination R^2 are forced through zero (Suzuki et al., 1994; Montel et al., 1996). Weighted average ages (Ma) with MSWD and minimal 2σ error are calculated from single analyses according to Ludwig (2001). The symbols mark analyses belong to distinct monazite age populations (ca. 30-70 Ma, BA 20-17; ca. 100-200 Ma, BA 11-18; ca. 120-250 Ma, BA 22-18; ca. 280-330 Ma, BA 20-17 and BA 22-17) that define isochrones. White square symbols mark data of low-Th monazites, not considered for isochrone weighted mean ages. Backscattered electron images (BSE) of monazite (b, c, e, f, h, i), showing single Th-U-Pb ages (Ma) and weighted averages with 2σ error calculated from several analyses within a grain. (a) BA 20-17, garnet micaschist, Challhuaco hill. (b) Monazite (Mnz) with Carboniferous ages. (c) Sponge-like monazite after strong alteration, situated in mica-rich domain with muscovite (Ms) and chlorite (Chl); weighted average age is calculated from low-Th analyses. (d) BA 20-17, garnet micaschist, Challhuaco hill. (e) Small monazite grain with low Th-contents in the upper part. Weighted average is calculated from lower part with 1-6 wt. % Th. (f) Small Jurassic monazite with weak oscillatory zonation pattern. (g) BA 11-18, paragneiss, Jakob lake. (h) Strongly sutured monazite grain surrounded by chlorite. (i) Small and strongly sutured monazite grains with muscovite and chlorite. Only monazite with total >98.5 wt. % of oxides are considered for weighted average age.

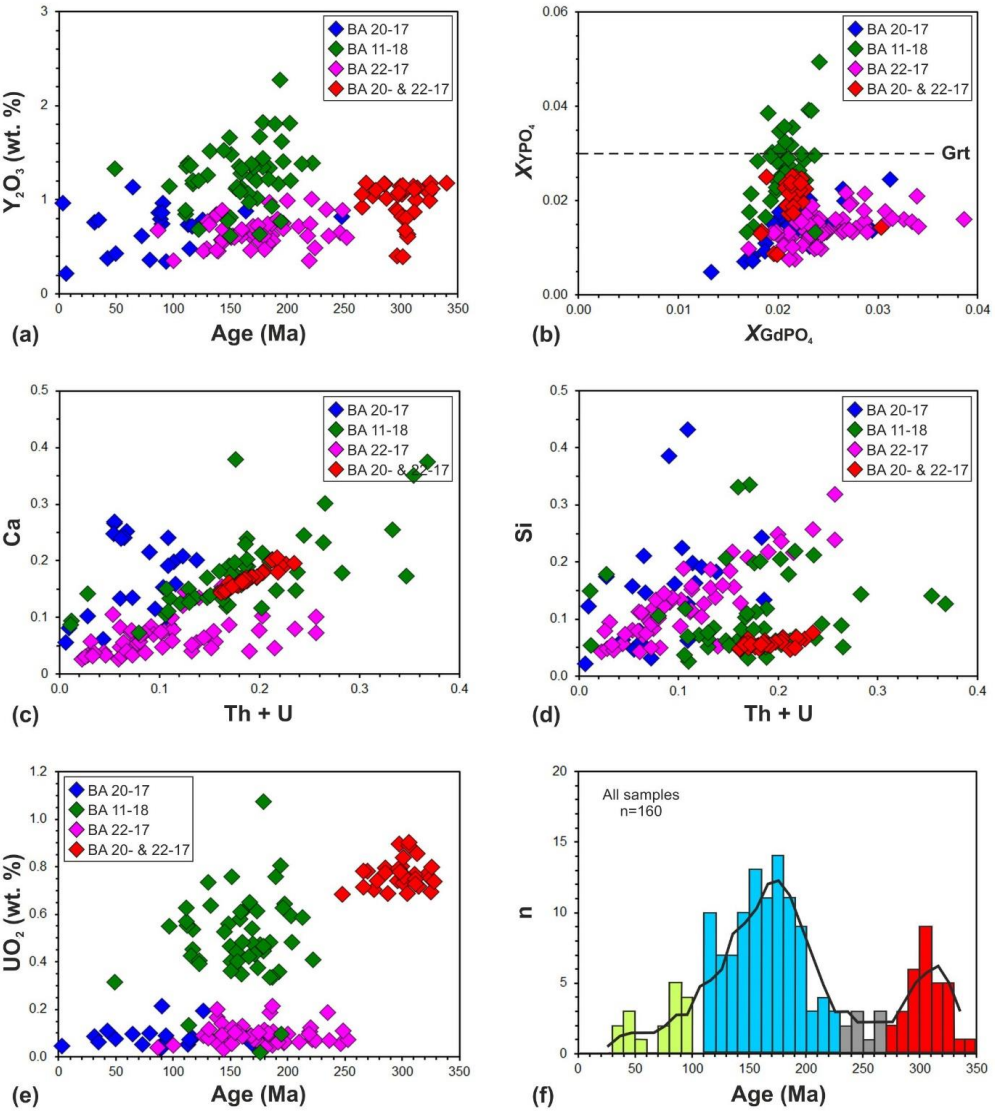

Fig. 8. Mineral chemistry and distributions of monazite Th-U-Pb chemical ages (see also Fig. 7). (a) Age vs Y_2O_3, showing elevated Y_2O_3 contents in sample BA 11-18. (b) X_{GdPO4} vs X_{YPO4} (mole fractions). Maximum X_{YPO4} in garnet (Grt) mineral zone according to Pyle et al. (2001). (c) Th+U vs Ca (mole fractions). (d) Th+U vs Si (mole fractions). (e) Age vs UO_2. (f) Histogram of monazite ages in all samples (BA 20-17, BA 22-17 and BA 11-18). Diverse distribution of Carboniferous, Jurassic and minor Cretaceous monazite populations.

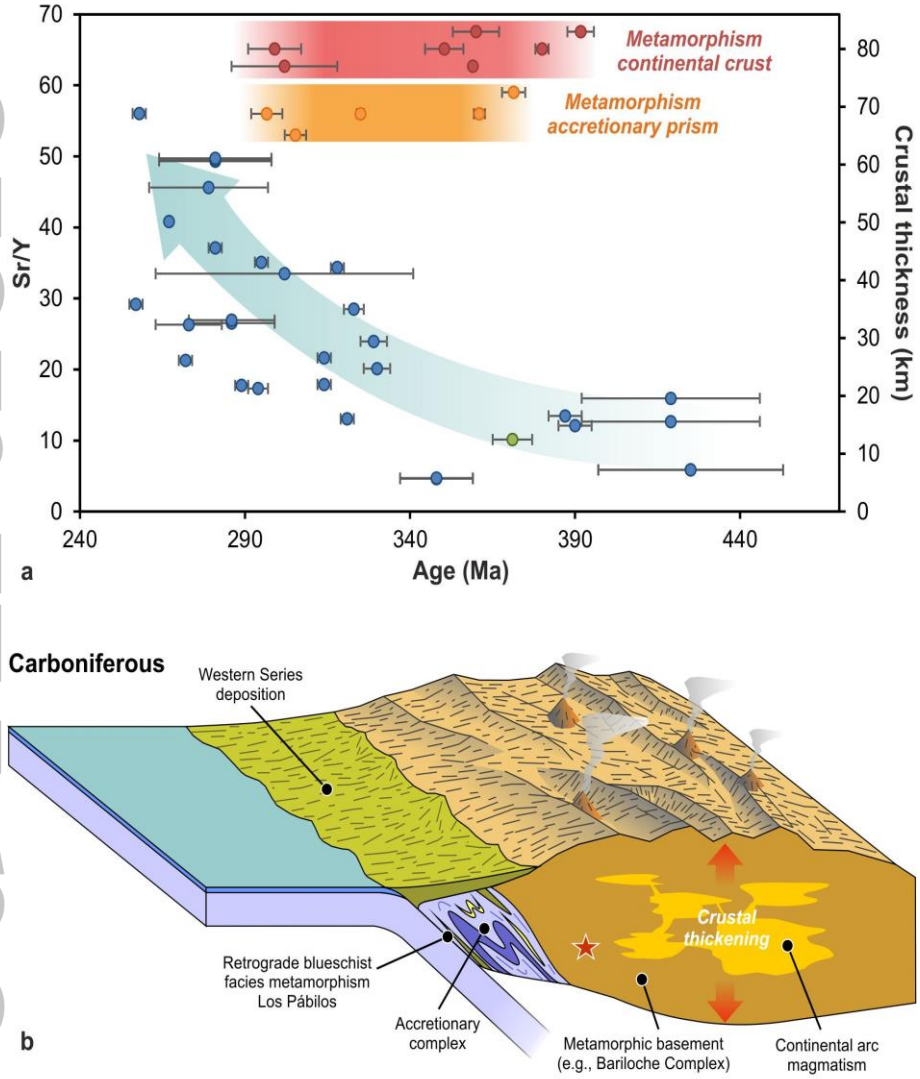

Fig. 9. (a) Compilation of Sr/Y and U-Pb zircon geochronologic data (Varela et al., 2005, 2015; Pankhurst et al., 2006) of intrusions of Argentina (blue), recording increasing crustal thickness of the Late Paleozoic continental arc. Equivalent crustal thickness values were estimated using the equation of Chapman et al. (2015). Data from a granitic clast (green) of a conglomerate in Chile, which is inferred to derive from the Devonian continental arc in Argentina (Quezada, 2015; Hervé et al., 2016), are included as well. The timing of metamorphism of metamorphic complexes of Argentina (red; Lucassen et al., 2004; Varela et al., 2005; Urraza et al., 2008; Martínez et al., 2012; this work) and accretionary prism complexes of Chile (orange; Willner et al., 2004; Kato et al., 2008; McDonough *apud* Quezada, 2015) is also indicated. (b) Schematic Carboniferous tectonic setting for the region south of ca. 40 °S (modified after Kato et al., 2008; Martínez et al., 2012; Hervé et al., 2013, 2016). Continental arc magmatism is recorded by Carboniferous intrusions distributed between the North Patagonian Cordillera and the western North Patagonian Massif (Varela et al., 2005, 2015; Pankhurst et al., 2006). In the accretionary prism (Chile), deposition of the Western Series sedimentary protoliths takes place (Hervé et al., 2013), whereas the Los Pábilos boulders undergo exhumation and retrograde blueschist facies metamorphism (Willner et al., 2004; Kato et al., 2008). The red star shows the location of the Challhuaco hill samples. See Section 5.2 for further details.

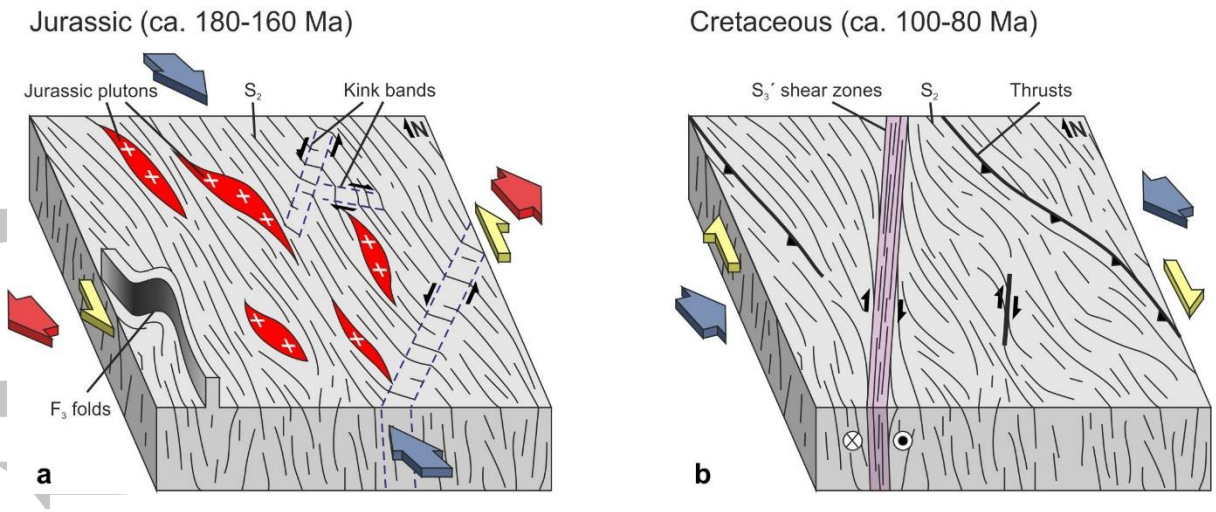

Fig. 10. Schematic Jurassic (a) and Cretaceous (b) structural evolution of the study area. Maximum shortening (blue arrows) and extension (red arrows) directions together with strike-slip component (yellow arrows) are indicated. See Section 5.3 for further details. (a) Emplacement of Jurassic magmatism and development of conjugated kink bands and F_3 open folds in a strike-slip-dominated transtensional setting (modified after Castro et al., 2011a). (b) Thrusting and dextral shearing related to dextral transpression.